Pernet-Fisher et al. (2026)
Impact resetting of the U-Pb, Pb-Pb, and Rb-Sr chronometers in the 4.3 Ga lunar granitoids
Advances in Geochemistry and Cosmochemistry 2(1): 771, https://doi.org/10.33063/agc.v2i1.771

Research article

Impact resetting of the U-Pb, Pb-Pb, and Rb-Sr chronometers in the 4.3 Ga lunar granitoids

John F. Pernet-Fisher[1] ✉ Katherine H. Joy[1] Josh F. Snape[1] Felix Boschetty[1]
Margaret E. Hartley[1] David A. Neave[1] Martin J. Whitehouse[2] Romain Tartèse[1]

[1] Department of Earth and Environmental Sciences, University of Manchester, Oxford Road, Manchester, M13 9PL, UK
[2] Department of Geosciences, Swedish Museum of Natural History, Stockholm, Sweden

✉ **Correspondence to:** John F. Pernet-Fisher: john.pernet-fisher@manchester.ac.uk

Author contributions: Conceptualization: JPF; KHJ. Funding Acquisition: KHJ. Investigation: JPF. Methodology: JPF; JFS; MJW; RT. Validation: JPF; KHJ; JSF; FB; MEH; DAN; MJW; RT. Visualization: JPF; KHJ. Writing – original draft: JPF. Writing – review & editing: JPF; KHJ; JFS; FB; MEH; DAN; MJW; RT.

Data, code, and outputs: Pernet-Fisher (2026) https://doi.org/10.48420/29126819.v2

Submitted: 2025-04-29
Accepted: 2026-04-02
Published: 2026-06-30

Production editor:
Ryan Ickert

Handling editor:
Nick Roberts

Reviews:
Two anonymous reviewers

Copyediting:
Elliot Carter,
Marthe Klöcking

Understanding when lunar granitoids formed remains a long-standing challenge hampering efforts to place these rock types into the wider context of the geological evolution of the Moon. In particular, it is poorly understood what their relationship is to KREEP-rich mafic lithologies such as alkali gabbronorites that have been linked to the generation of felsic melts through processes such as crustal underplating. Here we report *in situ* Rb-Sr, U-Pb, and Pb isotope systematics for lunar granitoid and alkali gabbronorite clasts from a range of Apollo landing sites. Our data indicate that the dates derived from the Rb-Sr, U-Pb, and Pb isotope systematics recorded by plagioclase, K-feldspar, Ca-phosphates, and glass most likely reflect impact resetting events rather than initial crystallisation ages. Granitoid and alkali gabbronorite samples 67975,9011, 14303,330, 72275,520, and 73255,9083 record dates consistent with the Imbrium impact event at 3.92 Ga, whereas samples 14305,111, 73235,73, and 14305,102 record modification by younger impacts at ~3.5 to ~3.6 Ga. Currently, zircon U-Pb isotope dates provide the most robust constraints on the formation ages of Apollo sampled granitoids. The majority of zircon dates are significantly older than those calculated from crater counting for lunar silicic domes (mostly between ca. 4 to 3.6 Ga). Consequently, it is not evident that mechanisms for generating large volumes of evolved melt by processes such as crustal underplating of mafic lithologies are needed. Formation within granophyre layers in magmatic layered intrusions or differentiated impact melt sheets cannot be ruled out.

1 Introduction

Understanding how felsic rocks formed on the Moon remains a long-standing challenge; this is in part due to their rarity and small sample size in existing collections. Rocks with felsic compositions make up only ~0.03 % of the mass of all Apollo samples (Seddio et al., 2013). These rock types are commonly referred to in the literature as granites; however, we prefer the term granitoid, as many reported fragments are not granites *sensu stricto* when considering their modal mineralogy. Granitoids are found at multiple Apollo (A) landing sites (A12, A14, A16, A17; e.g., Warren et al., 1983; Jolliff et al., 1991; Seddio et al., 2013; Valencia et al., 2024), within lunar meteorites (e.g., Fagan et al., 2014; Joy et al., 2011; Zeng et al., 2020; Oliveira et al., 2025), and at the farside Chang'e 6 landing site (Li et al., 2024; Zhang et al., 2025). These rock types typically occur as small (< 1 mm) clasts within breccias and soils. Their small size has made it challenging to employ geochronometers to constrain the timing of their formation and/or modification. Either clasts have been consumed by destructive analyses (e.g., Shih et al., 1994), or are required to have trace mineral phases such as zircon to perform *in situ* analyses (e.g., using the U-Pb chronometer; Meyer et al., 1996). Based largely on U-Pb isotope zircon dates, granitoid rocks display two date clusters between ~3.63 to 4.05 Ga and ~4.20 to 4.35 Ga (Meyer et al., 1996). However, the small number (~14) of samples with reported dates makes it unclear whether these represent continuous magmatism, distinct melting events, or whether some clasts have undergone impact (shock) modification and isotopic resetting.

Being able to differentiate between crystallisation and impact-related reset ages is important for placing these small rock fragments in the wider context of felsic melt generation on the Moon. It is unclear, for example, if these fragments relate to the large (estimated >10s km^3 volumes; Ivanov et al., 2016) silicic domes such as Gruithuisen, Hansteen, Mairan and Compton Belkovich. Notably, model crater counting ages for silicic domes have a smaller spread of ages (4.0–3.6 Ga; Wagner et al., 2002; Su et al., 2023) than Apollo granitoids. Deciphering the timing of granitoid formation is also important for placing constraints on their petrogenesis. Several scenarios have been proposed to account for evolved melt generation on the Moon. Models include differentiation of mantle partial melts rich in incompatible elements or differentiation within large impact melt ponds (Hurwitz and Kring, 2014; Shearer et al., 2022), potentially involving silicate liquid immiscibility (i.e., formation of coeval Fe-rich and Si-rich melts; Neal and Taylor, 1989; Jolliff et al., 1991). A popular model advocated in recent years is basaltic underplating (Hagerty et al., 2006; Gullikson et al., 2016; Valencia et al., 2024), which could produce melt on the scale needed to account for the silicic domes. Briefly, it has been observed in some terrestrial settings that, when magmas are intruded into mafic crust, the resulting heat can generate large volumes of felsic partial melts (Hagerty et al., 2006). Based on the observed trace element systematics of Apollo granitoids, experimental and modelling constraints indicate that, for this process to have occurred within the lunar crust, the source lithologies that underwent partial melting must have contained elevated concentrations of incompatible trace elements; e.g., they were KREEP basalts or their plutonic equivalents (Hagerty et al., 2006; Gullikson et al., 2016; Su et al., 2023; Valencia et al., 2024; Ravi et al., 2025). Here, KREEP refers to a geochemical component enriched in potassium (K), rare earth elements (REE), and phosphorus (P), relative to typical mare basalts.

A major limitation with the underplating formation mechanism is timing: dated Apollo KREEP basalts have younger formation ages (~3.85 to 4.15 Ga; Stöffler et al., 2006) than some granitoids. At face value, this appears to preclude the underplating formation mechanism as the source for the older group of granitoids; however, this age range for KREEP basalts is based on relatively few samples (three from Apollo 15 and one from Apollo 17; Stöffler et al., 2006; Shearer et al., 2023). Rock types such as alkali gabbronorites, which have been suggested to represent the mafic plutonic equivalents of KREEP basalts (Snyder et al., 1995), also have few reported dates (Shearer et al., 2023). One zircon U-Pb date (4.33 Ga; Meyer et al., 1989) is within range of the older group of granitoids; however, the host sample (67975,131) is a breccia, and it is unclear from the reported petrological context if the analysed zircon is situated within an alkali gabbronorite clast or is isolated within the breccia matrix.

There is a clear need to expand the range of crystallisation ages reported from lunar granitoids and KREEP-rich rock types in order to fully assess the role of crustal underplating as a granitoid formation mechanism. Different isotope systematics are modified differently by shock events/impact-gardening within the crust (e.g., Borg et al., 2005). Here, we report *in situ* Rb-Sr, U-Pb, and Pb isotope systematics for ten granitoid clasts (six of which do not have published isotopic data) and five alkali gabbronorite samples from a range of Apollo landing sites (A12, A14, A16, A17). We aim to establish whether these isotope systems can be used to place further constraints on granitoid and alkali gabbronorite formation ages, or whether the isotope systems have been modified by impact processes. The advantage of *in situ* measurements is that the petrographic context of the analysed phases is preserved. This aids in accurately interpreting the reported isotopic dates for the samples investigated here, and more widely within the literature.

2 Samples and Methods

For this study, we investigated granitoid clasts within breccias in 12013,13; 14305,111; 14305,102; 72275,520; 73235,73; 14304,209, and in polished sections of regolith breccia meteorite Northwest Africa (NWA) 4472 (described in Joy et al. 2011; see also pair NWA 4485; Arai et al. 2025). We also investigated granitoid fragments within soil samples 73255,9084; 73255,9083; 14303,330; and alkali gabbronorites clasts within breccias in 14304,278 and fragments within soil samples 14313,70; 67975,9011. Thin sections 14304,209 and 12013,13 are breccias that contain both granitoid and alkali gabbronorites clasts.

2.1 Scanning electron microscopy

Backscattered electron (BSE) and X-ray element maps were collected using a 15 kV acceleration voltage on a FEI QUANTA 650 field emission gun scanning electron microscope (SEM) equipped with a Bruker Quantax energy dispersive spectrometer (EDS) at the University of Manchester.

2.2 Major and trace element analyses

Mineral major and minor element chemistry was measured using a Cameca SX100 electron microprobe at the University of Bristol. Element abundances (Si, Al, Fe, Ca, Mg, Ti, Na, K, Mn, Cr, Ba) were measured with an accelerating voltage of 20 kV and a 20 nA beam current. Major element abundances for felsic phases (silica, plagioclase, alkali feldspar, and Si-K-rich glass) were measured with a defocused (10 µm) beam. Pyroxene was analysed with a fully focused beam. All sections were carbon coated prior to analysis. Counting times for each element were between 10 and 60 s, depending on element abundances. Typical analytical uncertainties were ~0.1 wt% for major elements and ~0.05 wt% for minor elements. Standard PAP corrections were applied. The instrument was calibrated using both natural and synthetic standards (Table S1, in Supporting Data; Pernet-Fisher, 2026). Additional high-precision analyses of Ti in silica for sample NWA 4472 were obtained using a Cameca SX100 electron microprobe at the

University of Manchester. Full details of this method can be found in the Supplementary Materials.

Trace element abundances were obtained using a Teledyne Analyte Excite+ 193 nm ArF Excimer laser ablation (LA) system equipped with a HelEx II active 2-volume ablation cell coupled to an Agilent 8900 inductively coupled plasma mass spectrometer (ICP-MS) at the University of Manchester. The NIST SRM 612 reference glass was used to tune the instrument, optimise signal intensities, and maintain low levels of oxide formation ($^{232}Th^{16}O/^{232}Th < 0.2\,\%$) and a $^{238}U/^{232}Th$ ratio close to unity. A summary of the analytical protocol is provided in Table S2 (Pernet-Fisher, 2026). Data were acquired for masses ^{31}P, ^{39}K, ^{45}Sc, ^{47}Ti, ^{51}V, ^{52}Cr, ^{55}Mn, ^{59}Co, ^{60}Ni, ^{85}Rb, ^{88}Sr, ^{89}Y, ^{90}Zr, ^{93}Nb, ^{137}Ba, ^{139}La, ^{140}Ce, ^{141}Pr, ^{146}Nd, ^{147}Sm, ^{153}Eu, ^{157}Gd, ^{159}Tb, ^{163}Dy, ^{165}Ho, ^{166}Er, ^{169}Tm, ^{172}Yb, ^{175}Lu, ^{178}Hf, ^{181}Ta, ^{208}Pb, and ^{232}Th. Minerals were ablated using a circular spot size ranging from 40 to 85 µm, this range reflecting the maximum spot size the minerals targeted could accommodate. Ablation was carried out in a helium atmosphere at a repetition rate of 5 Hz with the laser energy at the target (fluence) regulated at 5 J cm^{-2}. Ablation time lasted 40 s with 10 s intervals between analyses, which was used to establish instrument background counts for the measured species. The advantage of time-resolved analyses is that signals can be monitored for the ablation of inclusions. The trace element data reduction scheme of the Iolite v4 software (Paton et al., 2011) was used for data reduction. Glass standard BIR-1G was used as the primary calibration standard. Calcium was used as the internal normalising element. Repeat analyses of BCR-2G and BHVO-2G reference glasses were carried out over the sessions to assess data quality (Tables S3 and S4). Typical percent relative standard deviations (% RSD) for most elements range from 6 to 10 % across all standards. The calculated trace element abundances for the secondary standards are within ~10 % of the certified values reported within the GeoReM database (Jochum and Nohl, 2008) for most elements, and within 5 % for rare earth element (REE) abundances in BHVO-2G. Typical detection limits were less than 100 ng g^{-1}.

2.3 Rb-Sr isotopes

Rb-Sr isotope analyses were carried out using the same LA-ICP-MS instrument as used for trace element analyses. A summary of the Rb-Sr analytical protocol is provided in Table S5. Plagioclase, alkali feldspar, Ca-phosphate, and Si-K-rich glass were ablated in a helium atmosphere using a spot size of 50 µm (40 µm for Ca-phosphate), a fluence of 5 J cm^{-2}, and a repetition rate of 5 Hz. Each analysis lasted 60 s (40 s for Ca-phosphate) and was preceded by a 30 s counting time of the gas blank (background). Initial tuning of the ICP-MS and mass calibration was performed at the start of the analytical session in single quadrupole and no gas mode by optimising the ion signals during ablation of the NIST SRM 612 reference glass, while maintaining $^{238}U/^{232}Th$ close to unity and minimising the $^{232}Th^{16}O/^{232}Th$ ratio (< 0.2 %).

To resolve the isobaric interference between ^{87}Rb and ^{87}Sr, Sr isotopes (^{86}Sr, ^{87}Sr, ^{88}Sr) were analysed as oxides (^{102}SrO, ^{103}SrO, ^{104}SrO). This was done using the ICP-MS in triple quadrupole mode. In this mode, ions are filtered through the first quadrupole and enter a collision-reaction cell comprised of N_2O delivered at a flow rate of ~0.16 mL min^{-1} (corresponding to 15 % on the fourth mass flow controller of the Agilent 8900 ICP-MS) as Sr reacts effectively with N_2O (Hogmalm et al., 2017; Rösel and Zack, 2022), while Rb does not. We analysed ^{85}Rb on-mass instead of ^{87}Rb to avoid isobaric interference with any non-reacted ^{87}Sr, and used the natural $^{87}Rb/^{85}Rb$ ratio of 0.38562 to calculate ^{87}Rb abundances. Sensitivity obtained on NIST SRM 612 (35 µm raster, fluence of 5 J cm^{-2}, and repetition rate of 8 Hz) in triple quadrupole no gas mode and with the addition of 0.16 mL min^{-1} N_2O in the collision cell are reported in Table S5. All analyses with $^{88}Sr^{16}O$ intensities > 1.3×10^6 were filtered out as this is above the ICP-MS pulse-to-analogue (P/A) factor threshold, which cannot be tuned adequately in triple quadrupole mode.

For plagioclase, alkali feldspar, and Si-K-rich glass, we used NIST SRM 612 as the primary calibration standard for $^{87}Sr/^{86}Sr$ and $^{87}Rb/^{86}Sr$ ratios (using known ratios of 0.709 063 ± 0.000 020 and 1.160 ± 0.015, 2σ; GeoReM database; Woodhead and Hergt, 2001). Given that matrix mismatch between the primary standard and the analyte can result in significant Rb/Sr fractionation, we followed the approach of Bevan et al. (2021) whereby, at the start of each analytical session, we analysed plagioclase and alkali feldspar from the well-characterised Shap Granite (Cumbria, UK) to define an isochron. We then calculated a correction factor to adjust the measured $^{87}Rb/^{86}Sr$ values until the resulting isochron date matched the known age for Shap (394 ± 4 Ma, 2σ; Wadge et al., 1978; Pidgeon and Aftalion, 1978; Rundle, 1982). The resulting adjustment factors were then applied to all feldspar $^{87}Rb/^{86}Sr$ values.

To assess data quality, repeat analyses of reference glass BCR-2G (n = 50) and alkali feldspar pressed pellets (n = 80) FK-N and NIST SRM 70A (distributed by the CRGP and NIST, respectively) were carried out over the analytical campaign; our average $^{87}Rb/^{86}Sr$ and $^{87}Sr/^{86}Sr$ ratios are within uncertainty of previously reported data (Table S6; Figs S2 to S4). Percent relative standard deviation (% RSD at 2σ) for $^{87}Sr/^{86}Sr$ was 1.4 % for BCR-2G and SRM 70A, and 1.6 % for FK-N. For $^{87}Rb/^{86}Sr$, the % RSD was 5.3 % for BCR-2G; 9.4 % for FK-N; and 13.4 % for SRM 70A. The larger spread of measured $^{87}Rb/^{86}Sr$ ratios for the two FK-N and SRM 70A alkali feldspar pressed pellets likely reflects sample $^{87}Rb/^{86}Sr$ heterogeneity (Nebel and Mezger, 2006; Jegal et al., 2022; Redaa et al., 2023). Redaa et al. (2023) reported a similar % RSD (8.6 %) for their $^{87}Rb/^{86}Sr$ LA-ICP-MS/MS analyses of FK-N. We agree with Redaa et al. (2023) that these pressed pellets of feldspar are not suitable as primary calibration standards for *in situ* Rb/Sr dating. To further validate our analytical protocol, we analysed four terrestrial granites as unknowns, with published Rb-Sr ages ranging from 570 to 1632 Ma. Details of these samples are reported in the Supplementary Materials. For

these samples, we obtained Rb-Sr isochron dates consistent with their literature-reported ages (see Supplementary Text, Section S2). The full results of these analyses are reported in Table S7.

For Ca-phosphate analyses, we used BCR-2G as the primary calibration standard (using a known $^{87}Sr/^{86}Sr$ of 0.705 003 ± 0.000 080, 2σ; GeoReM database). To assess data quality, repeat (n = 8) analyses of reference apatite MRC-1 (Hou et al., 2013) and Durango (Apen et al., 2022) were carried out over the analytical campaign; our average $^{87}Sr/^{86}Sr$ ratios are within 2σ of previously reported data (Table S6). Percent relative standard deviation (% RSD at 2σ) for $^{87}Sr/^{86}Sr$ was 0.8 % for Durango and 0.9 % for MRC-1. Details of the analytical protocol are provided in Table S5 (column labelled session 8).

2.4 U-Pb and Pb isotopes

U-Pb and Pb isotopes were measured by secondary ion mass spectrometry (SIMS) using a Cameca IMS-1280 ion microprobe at the NordSIMS facility, Swedish Museum of Natural History, using analytical protocols similar to those in previous studies (e.g. Snape et al., 2016; Oliveira et al., 2025). A ~7–20 nA primary oxygen (O_2^-) ion beam was generated using an Oregon Physics Hyperion H201 radio-frequency plasma source. Prior to each measurement, an area of 20 µm × 20 µm was rastered for 50 s, which removed the carbon coating and minimised surface contamination. Care was taken for each analysis to ensure spots were isolated from adjacent material and cracks within the sample.

For the Pb isotope analyses, the magnetic field was regulated using a nuclear magnetic resonance field sensor. Isotopes ^{204}Pb, ^{206}Pb, ^{207}Pb, and ^{208}Pb were collected simultaneously on four low-noise (< 0.01 counts per second) electron multipliers. Background counts for each detector are reported in Table S8. For the U-Pb analyses, the Pb isotopes were collected using four electron multipliers as described above. Additionally, the magnetic field was varied such that an electron multiplier could be used to measure secondary ion beam intensities in a mass-switching sequence, which included matrix peaks for apatite ($^{40}Ca^{31}P^{16}O_4^+$), as well as $^{238}U^+$, $^{232}Th^{16}O^+$, $^{238}U^{16}O^+$, and $^{238}U^{16}O_2^+$.

To correct for instrumental mass fractionation and detector relative gain calibration, reference standards were analysed alongside our unknowns. Here, we used analyses of the USGS reference material BCR-2G ($^{206}Pb/^{204}Pb$ = 18.750, $^{207}Pb/^{204}Pb$ = 15.615, $^{208}Pb/^{204}Pb$ = 38.691; Woodhead and Hergt, 2000). Across the whole analytical session, reproducibility for BCR-2G was 0.18 % for $^{207}Pb/^{204}Pb$, 0.51 % for $^{206}Pb/^{204}Pb$, and 0.47 % for $^{208}Pb/^{204}Pb$ (Table S8; Fig. S5). For the gain correction, we divided the stated literature values by the corresponding average of each ratio obtained from all the BCR-2G analyses on a given day and multiplied the unknown measurements by the resulting correction factor. Measurements of the MPI-DING reference glass T1-G were also made and corrected using the same procedure as for the unknowns. The corrected T1-G values are all within 1.5 % of the recommended values (Jochum et al., 2011). For U-Pb measurements, sample Pb-U ratios were calibrated against the 2040 Ma BR5 apatite reference material with a $^{206}Pb/^{204}Pb$ ratio of > 1000 and U concentration of 68 µg g^{-1} (Kennedy et al., 2023) using a power law relationship between measured $^{206}Pb^*/U$ and UO/U. Data were processed using the using a suite of data reduction spreadsheets produced by Martin Whitehouse at the NordSIMS facility. The full results of these analyses are reported in Table S8.

2.5 Raman spectroscopy

Raman spectroscopy was carried out using a Horiba XploRA PLUS confocal Raman microscope at the University of Manchester. Spectra for silica were collected in spot analysis mode using a 532 nm wavelength laser and a 50× working distance objective to condense the laser beam down to ~1 µm. We measured a Raman Stokes shift range from 50 to 1300 cm^{-1}, with a spectral resolution of ~1 cm^{-1}. Spectra were background-corrected using the instrument software and compared with standard spectra for quartz, cristobalite, tridymite, and K-feldspar (orthoclase) from the RRUFF database (Downs and Denton, 2006). Background-corrected data are presented in Table S9.

3 Results

3.1 Petrography

Granitoids

Clasts and soil fragments investigated here range from ~200 µm to ~1 mm in size. Due to these small sizes, it is difficult to assess the extent to which the textures of individual fragments are representative of the rocks from which they were sourced. However, taken as a group, several common textural features can be observed (Fig. 1). Except for sample 12013,13, the granitoids studied here have crystal sizes > 100 µm, comprising silica (quartz and cristobalite have been identified, see Section 3.2), alkali feldspar, glass, and areas of micrographic intergrowths of alkali feldspar and silica (i.e., granophyre textures; e.g., Fig. 1b, c). Due to its fine-grained texture, sample 12013,13 has commonly been termed 'felsite' in the literature (Quick et al., 1982; Seddio et al., 2013). This sample is unique within breccias collected at the Apollo 12 landing site, and as such has been extensively described (e.g., Albee et al., 1970; Quick et al., 1982; Valencia et al., 2024). Briefly, this is a polymict breccia consisting of a glass that has elevated REE concentrations relative to the mafic and 'felsic' components that dominate the matrix (Fig. S1, Supplementary Materials). Samples 14305,111, 14303,330, 14304,209, and 14305,102 also contain Si-K-rich glass.

Within sample 14305,111, the Si-K-rich glass mantles the granitoid clast and contains a large (> 200 µm) relict cristobalite grain (Fig. 1h). Within sample 14305,102, a Si-K-rich glass patch is present within the host breccia matrix, containing numerous relict silica grains (Fig. 1e). Similarly, sample 14303,330 contains numerous Si-K-rich glass patches that contain relict silica, plagioclase, and K-feldspar (Fig. 1d). These glass patches have irregular

boundaries with the adjacent breccia matrix, filling gaps between grains and, in some cases, incorporating matrix minerals along the margins of the glass. Sample 14304,209 contains a ~700 µm patch of glass with a large (> 200 µm) relict silica grain (Fig. 1l). In contrast to 14305,102 and 14303,330, this glass patch has well-defined edges with its adjacent breccia matrix. Additionally, cracks or fractures within the glass are filled with pyroxene veins 10 to 20 µm wide. These might represent brittle fractures that have been subsequently filled by mafic melt. In contrast, sample 12013,13 does not contain Si-K-rich glass. Rather, we note that the felsic portion (characterised by needle-shaped silica set within K-feldspar) is texturally similar to the occurrence of Si-K-rich glass described in the samples above. That is, the felsic region forms a large irregular patch that surrounds larger (> 1 mm) clasts within the thin section (Fig. 1j), and in some cases incorporates matrix minerals that are chemically consistent with alkali suite compositions (Fig. 1k). Within the felsic regions some larger (> 100 µm) rounded silica grains are present that could represent relict grains from a precursor granitoid.

Reported accessory phases for Apollo granitoids commonly include Ca-phosphates (apatite and merrillite) and zircon (Meyer et al., 1996; Seddio et al., 2013). Within the samples investigated here, small (< 10 µm) zircon and Ca-phosphates are present in 14305,102 and NWA 4472, whereas only Ca-phosphates are observed in samples 73255,9083 and 14305,111.

Alkali gabbronorites

This rock type is present in samples 14304,278 and 12013,13 as large (> 1 mm) clasts within breccias (Fig. 1m and Fig. S1), whereas 14313,70 and 67975,9011 consist of small < 500 µm fragments within a coarse soil sample sub-split (Fig. 1n,o). Section 14304,278 contains three breccia chips. Clasts and fragments investigated here are made up of plagioclase and pyroxenes that range in size from ~200 to ~750 µm. All samples except 12013,13 display accessory silica, alkali feldspar, and Si-K-rich glass that occurs along plagioclase and pyroxene grain boundaries. For the samples investigated here, 14313,70 contains Ca-phosphates, and samples 14304,278 and 12013,13 both contain Ca-phosphates and zircon.

3.2 Major and trace element chemistry

Major and trace element systematics for all mineral phases and glass are reported in Tables S10 and S11. The compositions of plagioclase in the granitoids and alkali gabbronorites span similar An (molar Ca/[Na+Ca+K]) contents of 49.5 to 90.1 and 53.7 to 93.1, respectively (Fig. 2). For all samples except 14313,70, CI chondrite-normalised (Anders and Grevesse, 1989) plagioclase REE patterns (Fig. 3a,b) display strong LREE enrichments ($[La/Sm]_{CI}$ = 2.6 to 15.2) and have positive Eu anomalies (Eu/Eu*) that range from 5.35 to 114. Sample 14313,70 has a plagioclase with higher REE abundances than all other samples reported here (e.g., Nd_{CI} = 69.4 and Dy_{CI} = 31.2 vs. an average of Nd_{CI} = 11.0 and Dy_{CI} = 4.1 for other samples). Additionally, plagioclase in this sample displays a flatter LREE profile ($[La/Sm]_{CI}$ = 1.4) and a smaller Eu anomaly (Eu/Eu* = 2.51) than all other plagioclase reported here.

The alkali feldspar compositions reported across all samples are K-rich with Or contents (molar K/Na+Ca+K) > 95, except in 12013,13, which has Or contents from 70 to 80, reflecting a higher Na content (Fig. 2). Notably, the alkali feldspars extend to high BaO abundances, ranging from 0.54 to 5.3 wt% BaO (Table S8). The REE patterns of alkali feldspar are characterised by a strong enrichment of the LREEs relative to chondrite abundances ($[La/Sm]_{CI}$ = 4.2 to 62), pronounced positive Eu anomalies (Eu/Eu* = 276 to 968), and depletions of MREE and HREE relative to plagioclase (Fig. 3c).

Most samples (14304,278, 12013,13, 14305,111; 14305,102, 72275,520, 67975,9011, 14303,330, and 73255,9083) display so-called ternary feldspar compositions that lie within the miscibility gap of the albite-anorthite-orthoclase (Ab-An-Or) system (Fig. 2). Such compositions have previously been documented in other Apollo granitoids (Ryder et al., 1975; Simon et al., 2020; Valencia et al., 2024; Erickson et al., 2024), and potential causes for their genesis are discussed in Section 4.1.2. These feldspars display REE patterns similar with those in plagioclase (Fig. 3d), despite being in some cases significantly more K-rich (up to Or_{90}) and, therefore, more similar in major element composition to alkali feldspars. Both plagioclase and alkali feldspar display positive Yb anomalies (except in sample 14313,70). Ternary feldspars range from positive Yb anomalies to no enrichments in Yb relative to other HREE. Such a signature has been reported in plagioclase in other lunar highland lithologies (e.g., Haskin et al., 1982; Pernet-Fisher et al., 2024) and likely indicates the incorporation of Yb^{2+} over Yb^{3+} into feldspar due to the low fO_2 (< IW −1) typically recorded in lunar magmatic systems.

All Apollo alkali gabbronorites investigated here contain both low-Ca and high-Ca pyroxene. Additionally, orthopyroxene is reported in sample 14304,278 (Table S8; Fig. 4). Pyroxene Mg# (molar Mg/[Mg+Fe]) across the samples investigated here ranges from 63.8 to 76.8. Mineral phases within alkali gabbronorite clasts have chemistry that is distinct relative to other highland lithologies (i.e., Mg-suite and ferroan anorthosites). This is evident on plots of plagioclase An content vs. Mg# in mafic minerals (Fig. 5), where the studied clasts are consistent with high alkali suite compositions.

Tables S10 and S13 report the major and minor element chemistry of silica polymorphs. Notably, Al_2O_3, FeO, and TiO_2 extend to abundances > 0.1 wt%, similar to values reported for Apollo 12 granitoids (Seddio et al., 2015). Raman spectra were used to establish which silica polymorphs are present within the Apollo granitoid samples (Table S9, Fig. S11). Quartz is present in all samples except for 14305,111, which contains a large (~200 µm) cristobalite grain that does not form part of the quartz/feldspar granophyric intergrowth (Fig. 1h).

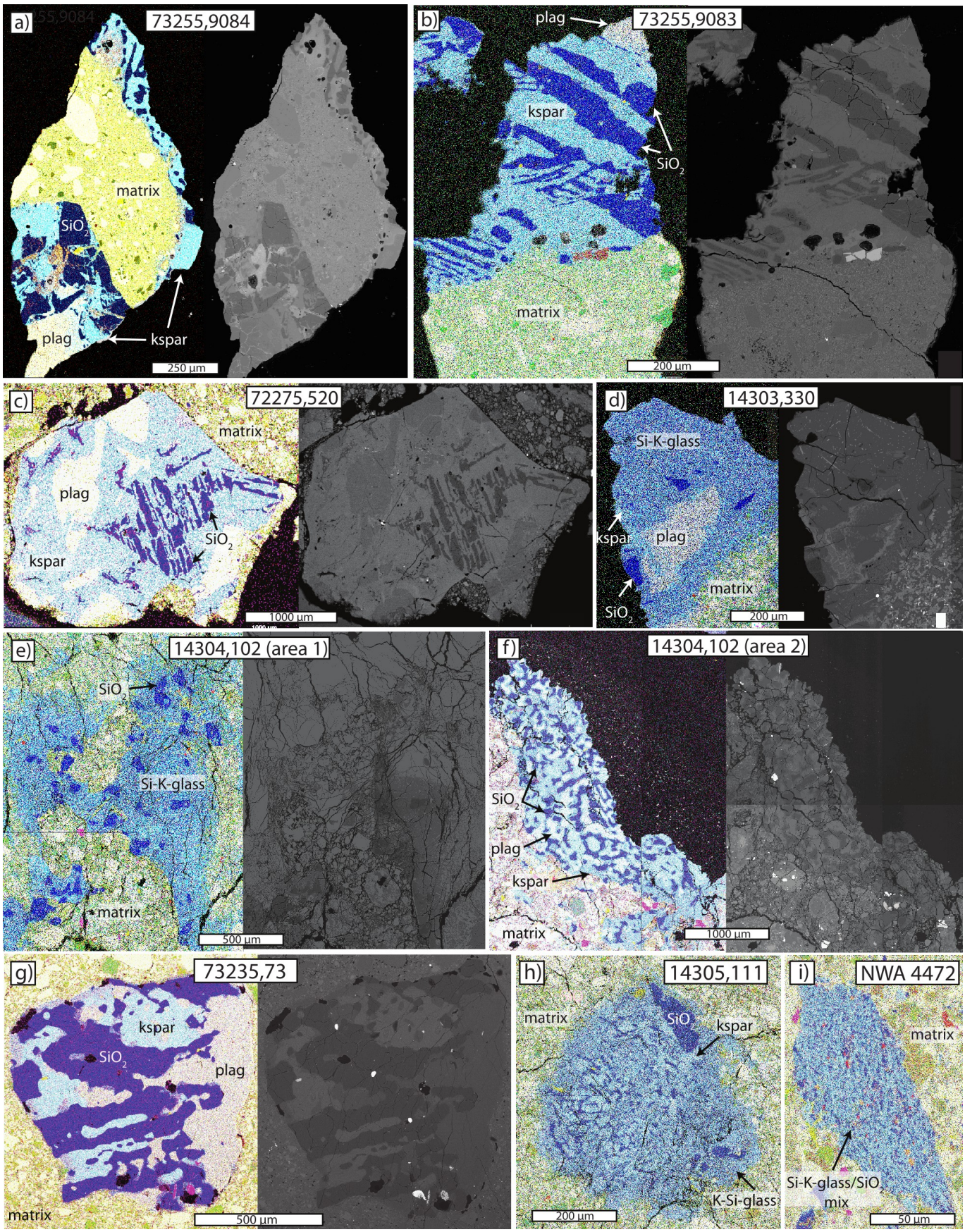

Figure 1. Back-scattered electron images and EDS false-colour element maps showing representative textures and minerals in the granitoid clasts investigated for this study. Colour scheme for combined element maps is: Mg = green, Al = white, Si = blue, K = cyan, Ca = yellow, Ti = pink and Fe = red. Plag = plagioclase; pyx = pyroxene; k-spar = K-feldspar; SiO_2 = silica. (continued overleaf)

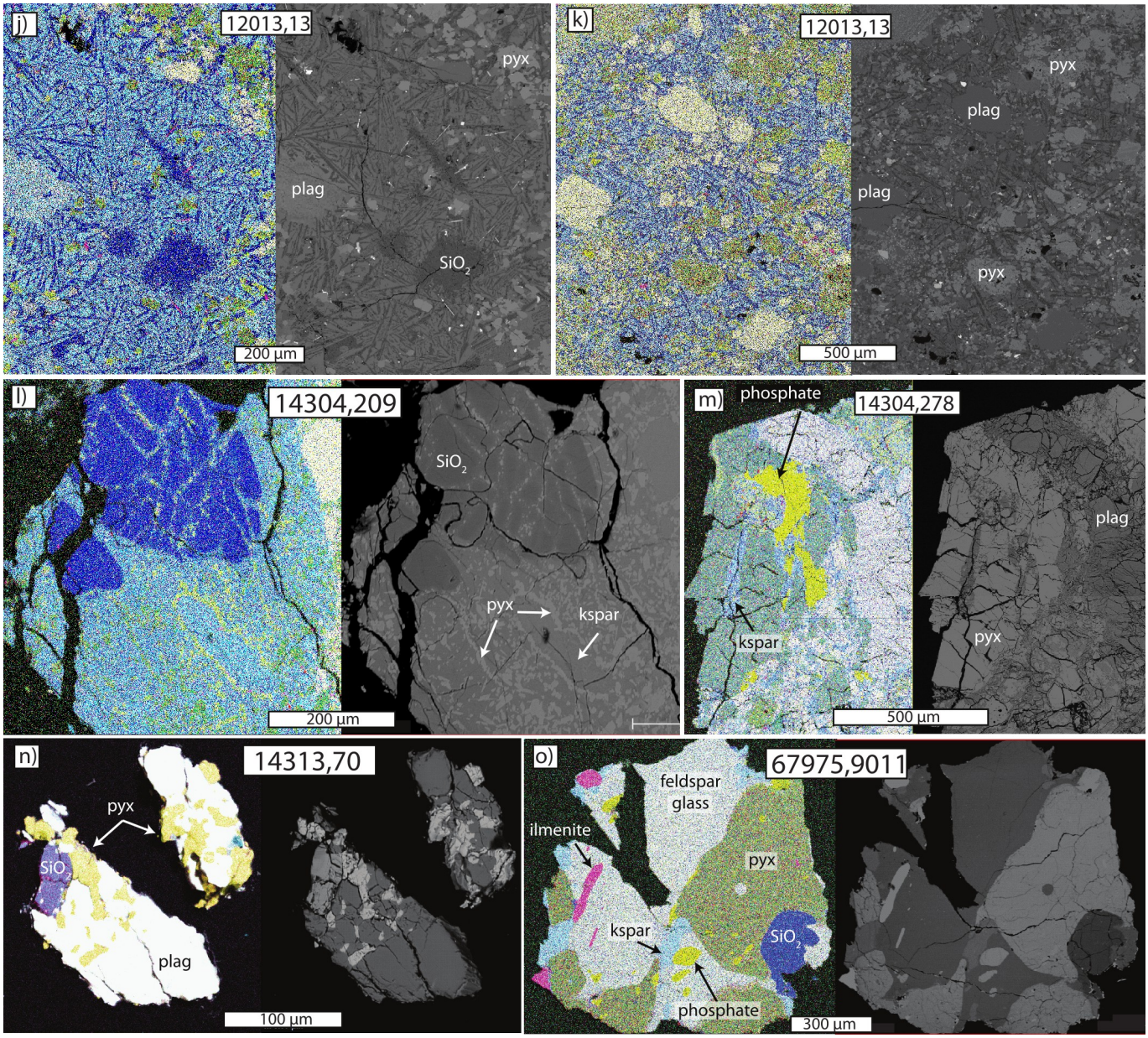

Figure 1. (continued)

There are two types of glass (where glass is defined as amorphous regions that are isotropic when observed in thin section under cross-polarised light). The first type is compositionally within range of the plagioclase and alkali feldspar compositions reported here; however, the calculated stoichiometry is not quite correct for feldspars (i.e., total cations of 4.9 rather than 5.0 per 8.0 oxygens). On a per-analysis basis, this reflects lower Na and K relative to stoichiometric feldspars. The second type is compositionally distinct from the mineral phases within these rocks. It displays high SiO_2 (67.0 to 79.5 wt%) and K_2O (6.99 to 12.94 wt%) abundances, so we refer to this glass as Si-K-rich glass. The composition of this glass is distinct from the reported major element bulk-rock compositions of most Apollo granitoids and is similar to the K-rich glass reported within mare basalt mesostasis regions and as melt inclusions within minerals (Potts et al., 2016; Zeng et al., 2020; Roedder and Weiblen, 1970; Pernet-Fisher et al., 2014, Fig. 6). In general, the Si-K-rich glasses from both the granitoids (red symbols) and alkali gabbronorites (purple symbols) overlap in composition. However, there are some differences: glass from the alkali gabbronorites extends to lower K_2O and BaO and higher TiO_2 and Al_2O_3 abundances for a given SiO_2 abundance (Fig. 6).

These glasses are typically enriched in incompatible elements (REE abundances ~100× chondrite; Fig. 3e, f). Glass in sample 14304,209 has REE abundances that are within the range of high-K KREEP (Warren, 1989). However, whereas high-K KREEP has a depletion of HREE with increasing atomic number relative to chondrite abundances ($[Dy/Yb]_{CI}$ = 1.2), both 14304,209 and 14305,102 display enrichments in HREE with increasing atomic number relative to chondrite abundances ($[Dy/Yb]_{CI}$ = 0.52 to 0.89). This pattern is commonly referred to as 'V' shaped and is reflected in bulk-rock REE profiles for Apollo granitoids (Warren et al., 1987). No REE data for Si-K-rich glass from

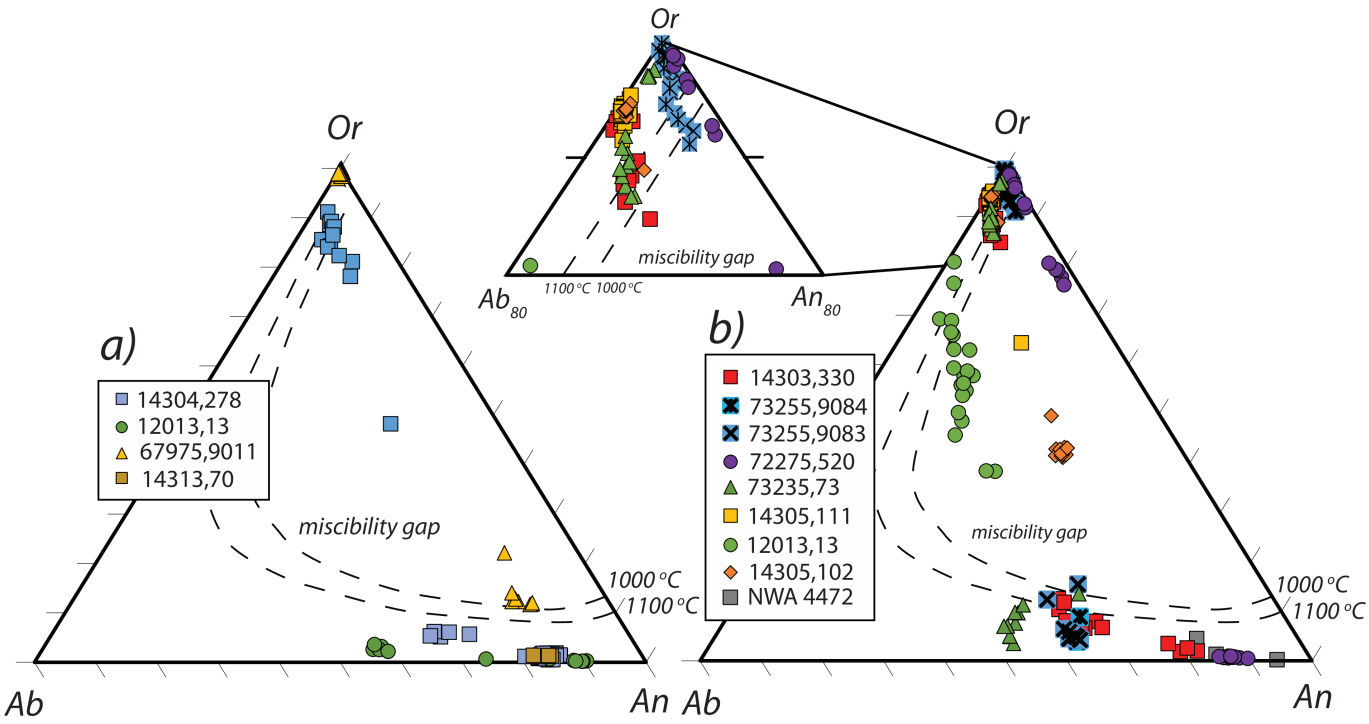

Figure 2. Or-Ab-An feldspar ternary plot for a) alkali gabbronorite clasts and b) granitoid clasts. The miscibility gap is for melts at temperatures of 1000 °C and 1100 °C at 1 kbar (~25 km lunar crustal depths; Fuhrman and Lindsley, 1988). At lower pressures, the feldspar stability field would get smaller.

mesostasis regions are available for comparison; however, LREE abundances for Si-K-rich glass inclusions within zircons are significantly lower (Ce_{CI} = 3.86; Zeng et al., 2020). Apollo granitoids have some of the highest bulk-rock Th abundances reported from lunar lithologies (up to 66 µg g^{-1}; Papike et al., 1998), resulting in $[Th/Sm]_{CI}$ values higher than high-K KREEP (K-KREEP = 2.2; Warren, 1989), the cause of which remains enigmatic (Korotev et al., 2003; Pernet-Fisher et al., 2024). The Si-K-rich glass reported here displays $[Th/Sm]_{CI}$ within the range of reported bulk rock ratios, extending from 5.4 to 41.

3.3 Rb-Sr geochronology

Plagioclase, alkali feldspar, and Si-K-rich glass (when present) were targeted for Rb-Sr isotope analysis. Results are reported in Table S12. Isochron dates were calculated using the IsoplotR programme (Vermeesch, 2018) and are summarised in Figures 7, 8, and 9 and Table 1. We used the ^{87}Rb decay constant reported by Villa et al. (2022). All reported uncertainties are 2σ. In some cases, the MSWD for the calculated isochrons is >2, potentially indicating isotopic disturbances in the phases analysed. The implications of this are discussed in Section 4.3.

For granitoid samples NWA 4472, 72275,520, 73235,73, 73255,9083 and alkali gabbronorite sample 14304,278, isochrons were plotted using plagioclase and K-feldspar analyses. Dates of 4140 ± 104 Ma, 4011 ± 157 Ma, 3661 ± 236 Ma, 3766 ± 155 Ma, and 3731 ± 649 Ma were calculated for each sample, respectively (Figures 7 and 8). Sample 14304,209 (that consists of only Si-K-rich glass) yields a date of 4442 ± 63 Ma, and alkali gabbronorite sample 67975,9011 yields a maskelynite/Ca-phosphate date of 3940 ± 188 Ma (Figure 8). Isochrons from all these samples yield initial Sr isotope ratios ($^{87}Sr/^{86}Sr_0$) that either fall within the uncertainty of, or exceed, the isotopic growth curve from the lunar initial value ($^{87}Sr/^{86}Sr > 0.698970$; Taylor, 1982).

For granitoid samples 14305,111, 14303,330, and 14305,102, both plagioclase and K-feldspar (blue symbols in Fig. 9) and Si-K-rich glass (red symbols in Fig. 9) were measured for Rb-Sr isotopes. Figure 9 displays both the plagioclase/K-feldspar isochrons (black lines) and Si-K-rich glass isochrons (red lines). For sample 14303,330, the date calculated from the plagioclase/K-feldspar isochron (3997 ± 130 Ma) is within the uncertainty of the date calculated from the Si-K-rich glass isochron (3965 ± 45 Ma). For samples 14305,111 and 14305,102 plagioclase/K-feldspar isochrons yield younger dates than those calculated from the Si-K-rich glass isochrons (3551 ± 129 Ma vs. 4005 ± 83 Ma for 14305,111 and 3523 ± 337 Ma vs. 4237 ± 92 Ma for 14305,102). Notably, for all three samples, the Si-K-rich glass isochrons yield initial Sr isotope ratios that are consistently lower than those yielded by the plagioclase/K-feldspar isochrons (Table S12, Fig. 9). If the Si-K-rich glass isochrons are anchored using the initial Sr isotope ratio calculated using the plagioclase/K-feldspar isochrons, the resulting dates are within 2σ of the unanchored Si-K-rich glass dates (Fig. S13). The potential causes for the differences between the Si-K-rich isochron dates vs. plagioclase/K-feldspar isochron dates are explored in Section 4.3.

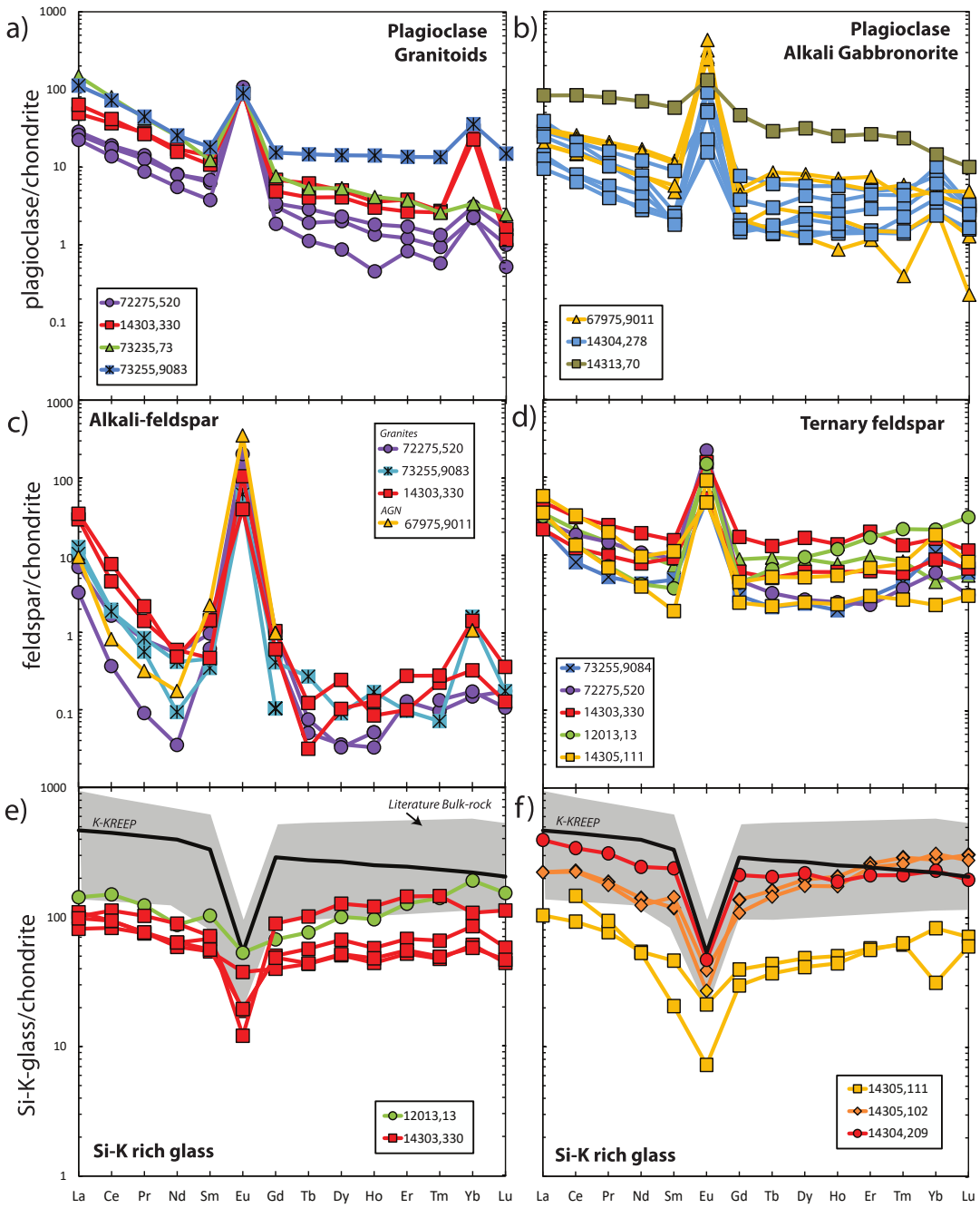

Figure 3. CI chondrite-normalised REE abundances for plagioclase (a,b), alkali feldspar (c), ternary feldspar (d), and Si-K-rich glass (e,f). Chondrite normalising values from Anders and Grevesse (1989). Literature Apollo granitoid bulk rock values from Seddio et al. (2013) and references therein; high-K KREEP values from Warren (1989).

3.4 Pb-Pb geochronology

All U-Pb and Pb-Pb data are reported in Table S8 and are summarised in Table 1. All reported uncertainties are 2σ.

In many crystalline igneous lunar samples, Pb-Pb isotopic compositions of minerals such as plagioclase, K-feldspar, and glass can be interpreted as mixtures between three components: (1) an initial Pb component (the Pb isotope composition of common Pb at the time of crystallisation); (2) a radiogenic Pb component that is result of radiogenic growth from the initial Pb; and (3) terrestrial contamination introduced during sample preparation, coating, and handling (Snape et al., 2016). This assumption is valid provided that the Pb in a sample was derived from a single magmatic source and was not lost due to, for example, heating of the rock. In this case, analyses in $^{207}Pb/^{206}Pb$ vs. $^{204}Pb/^{206}Pb$ space will plot within a triangular mixing array defined by these three components, the isochron being defined by the tie-line between the initial and radiogenic Pb components (i.e. the left-hand edge of this mixing array). This method for defining a Pb-Pb isochron is well established and has been detailed previously (e.g. Snape et al., 2016, 2019; Che et al., 2021; Li et al., 2021; Snape et al., 2024; Joy et al., 2024).

We follow the approach of Snape et al. (2016), filtering data with the highest $^{204}Pb/^{206}Pb$ values to define a series of analyses that likely reflect the left-hand edge of such

Table 1. Summary of dates reported (in Ma). Uncertainties are 2σ. *maskelynite/k-spar date.

	plag/K-spar/glass dates			phosphate dates			plag/K-spar dates			Si-K-rich glass dates		
Sample	Pb-Pb	±	MSWD	Pb-Pb	±	MSWD	Rb-Sr	±	MSWD	Rb-Sr	±	MSWD
	Ma	Ma		Ma	Ma		Ma	Ma		Ma	Ma	
Granitoids												
14305,102	3956	19	1.6				3523	337	1.3	4237	92	2.2
14303,330	3918	18	1.2				3997	130	3.4	3965	45	13
14304,209										4433	64	1.4
14305,111							3551	129	4.7	4005	83	2.1
73235,73	3605	223	0.78				3661	236	1.8			
73255,9084	3735	45	1.22									
73255,9083	3889	107	1.5				3766	155	4.1			
72273,520							4011	157	29			
NWA 4472							4140	104	2.9			
Alkali gabbronorites												
67975,9011	3566	3	1.7				3940*	188	1.3			
14304,278				3915	11	0.53	3731	649	0.41			
14313,70				3939	11	0.18						

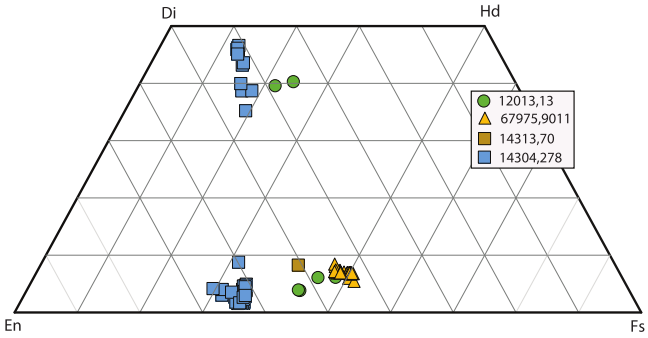

Figure 4. Pyroxene quadrilateral for the Apollo 12, 14, and 16 alkali gabbronorite samples.

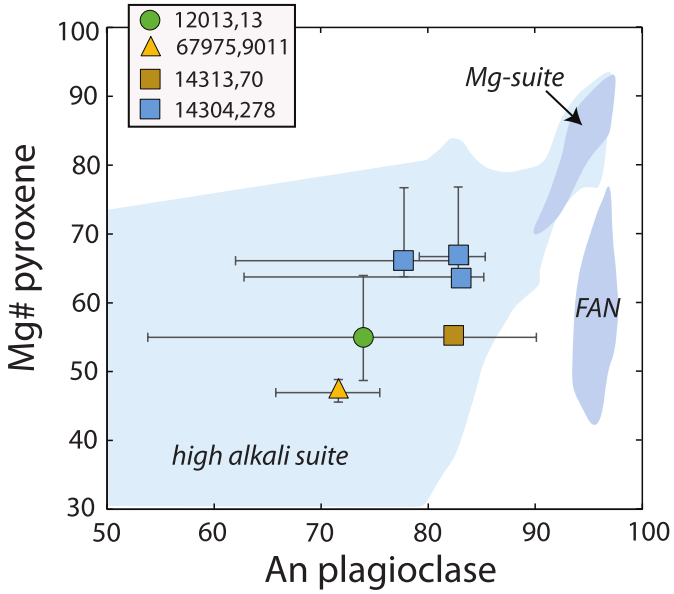

Figure 5. Average Mg# in pyroxene vs. An in plagioclase for Apollo alkali gabbronorites. Bars represent the min and max range of An and Mg# values observed in each clast. Blue representing the range of compositions for highland lithologies are from Yamaguchi et al. (2010).

a mixing array (Pb isotope ratios are plotted in Figs 10 and 11). The regression through these analyses can then be used to calculate a date for each sample. However, it is important to note that the complicated nature of the granitoid samples studied here (i.e., petrologic indications of impact modification) together with their small size limiting the number of analyses that could be measured per clast, raises the distinct possibility that the left-hand edge of the mixing array may not represent a true sample isochron.

In many cases our analyses display a spread of $^{204}Pb/^{206}Pb$ (Figs 10 and 11), likely reflecting contamination by modern terrestrial Pb (Stacey and Kramers, 1975). Therefore, it is important to note that the analyses used to define the left-hand mixing array could still reflect a Pb isotope composition affected by terrestrial contamination, which would result in an inaccurate date. This is particularly the case for samples where the clast size was such that only relatively low numbers of analyses could be made (e.g., n < 10; 73255,9084 and 14305,102). Additionally, if Pb loss had occurred and the isotope system were reset (either partially or fully) then the most radiogenic Pb isotope composition measured (i.e., with the lowest $^{204}Pb/^{206}Pb$ and $^{207}Pb/^{206}Pb$) would provide a lower limit for the original crystallisation age of the rock and an upper limit for the time at which the Pb loss occurred. For example, if an analysis yields a radiogenic $^{207}Pb/^{206}Pb$ ratio equating to a $^{207}Pb/^{206}Pb$ date of 3922 Ma (i.e., the date interpreted to be the Imbrium basin-forming event), then the rock must have crystallised by this time, and any impact that reset the isotope system in the sample could not have occurred any earlier.

Table 1 reports the Pb-Pb isotope dates for the samples using the method described. Given the potential complications identified above and assuming the samples studied here

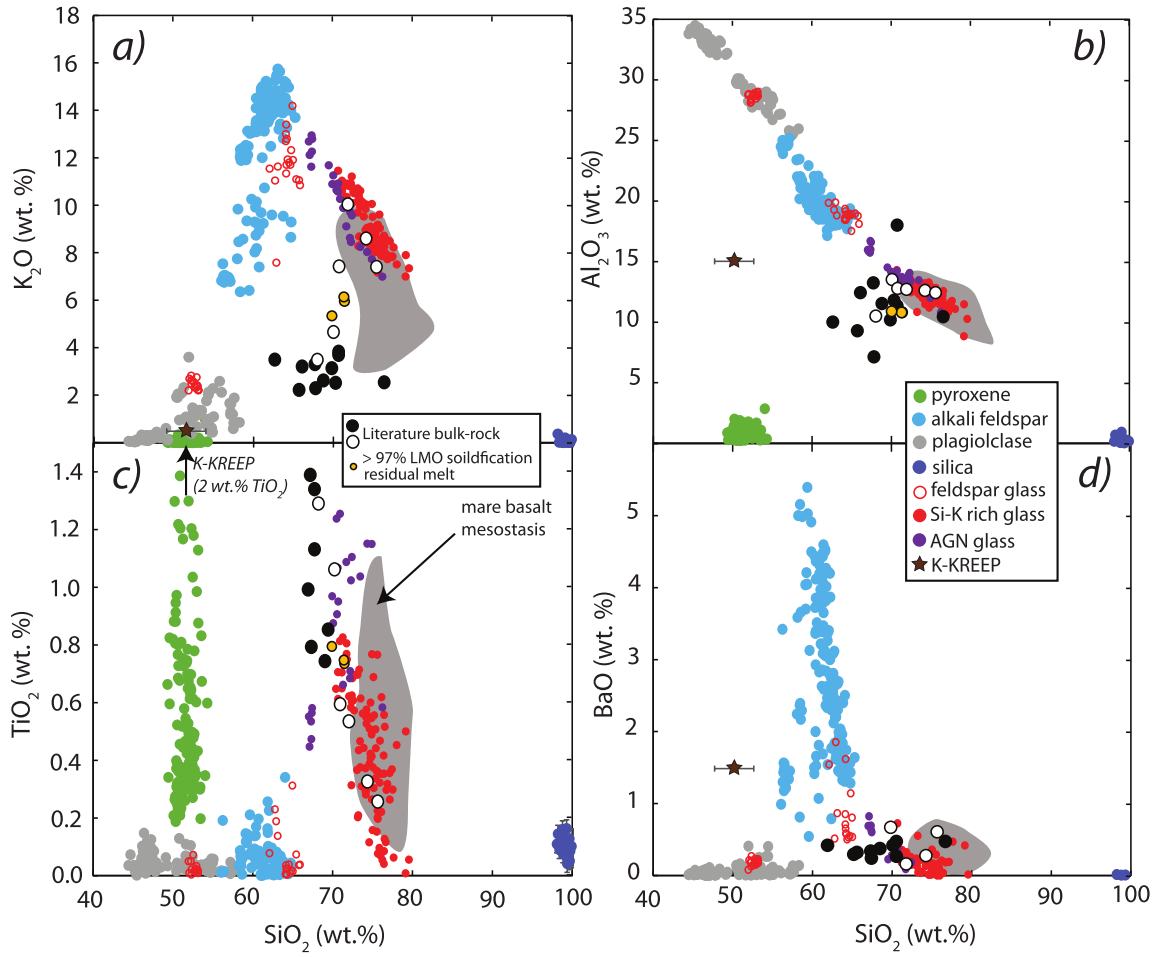

Figure 6. K_2O, TiO_2, Al_2O_3, and BaO vs. SiO_2 for Si-K-rich and feldspar glass (red and purple circles). For context, chemistry of Apollo granitoid mineral phases are plotted: pyroxene – green circle; alkali feldspar – cyan circle; plagioclase – grey circle; silica – blue circle. Black symbols and white symbols are reported bulk rock analyses for Apollo granitoids (Seddio et al., 2013). Only six fragments have had SiO_2 measured directly (white symbols). The SiO_2 for the remaining samples is estimated using the correlation between TiO_2 and SiO_2 (see Fig. S12). Yellow symbols represent the composition of silicate liquid immiscible (SLI) Si-rich glass in lunar magma ocean (LMO) crystallisation experiments (Zhang et al., 2024). The grey fields represent the range of mesostasis glass compositions in mare basalts (Roedder and Weiblen, 1970, 1971; Warner et al., 1978; Pernet-Fisher et al., 2014; Potts et al., 2016; Zeng et al., 2020). High K-KREEP value is from Warren (1989).

reflect a single-stage U-Pb history, these dates represent our best estimate for the Pb-Pb isotope ages of these samples.

Samples yield a range of dates from 3918 ± 18 Ma to 3566 ± 3 Ma. The most robust regression is identified for 14303,330 (Fig. 10a; 3918 ± 18 Ma; MSWD = 1.2; n = 30). By contrast, the regressions identified for samples 73255,9083, 73255,9084 and 73235,73 are poorly defined, comprising only three or four points each. However, it is notable that these samples yield Pb-Pb dates that are within the uncertainty of the equivalent *in situ* Rb-Sr dates reported above (Table 1). Plagioclase analyses from 14305,102 display strong terrestrial Pb contamination with five analyses defining a clear mixing trend between our calculated isochron and terrestrial Pb (Fig. 11a). This means it is not possible to robustly calculate a plagioclase/K-feldspar date. A regression through the left-most analyses for sample 14305,102 yields an intermediate age (3956 ± 19 Ma) between the *in situ* Rb-Sr plagioclase/K-feldspar (3523 ± 337 Ma) and Si-K-rich glass (4237 ± 92 Ma) dates (Fig. 11b). Out of a total of 22 feldspar analyses in alkali gabbronorite 67975,9011 (Fig. 10d), a robust regression is defined by 19 points (MSWD = 1.4). The remaining three points plot to the right of this line and are filtered out due to likely terrestrial contamination. If taken to represent an isochron, this regression would indicate a date of 3567 ± 3 Ma.

No meaningful date was calculated for sample 12013,13 (Fig. 12d). While this sample displays analyses that trend towards terrestrial Pb isotope compositions, the left-hand edge of the mixing triangle forms an isochron that is older than the age of the Solar System (Fig. 12d). As noted previously, this sample consists of a number of different clasts. Each of these clasts may have its own, distinct Pb isotope mixing triangle with terrestrial Pb. Therefore, our analyses could reflect a mix of multiple different Pb components associated with each clast, rather than the assumed three-component mixture of the felsic area. Given

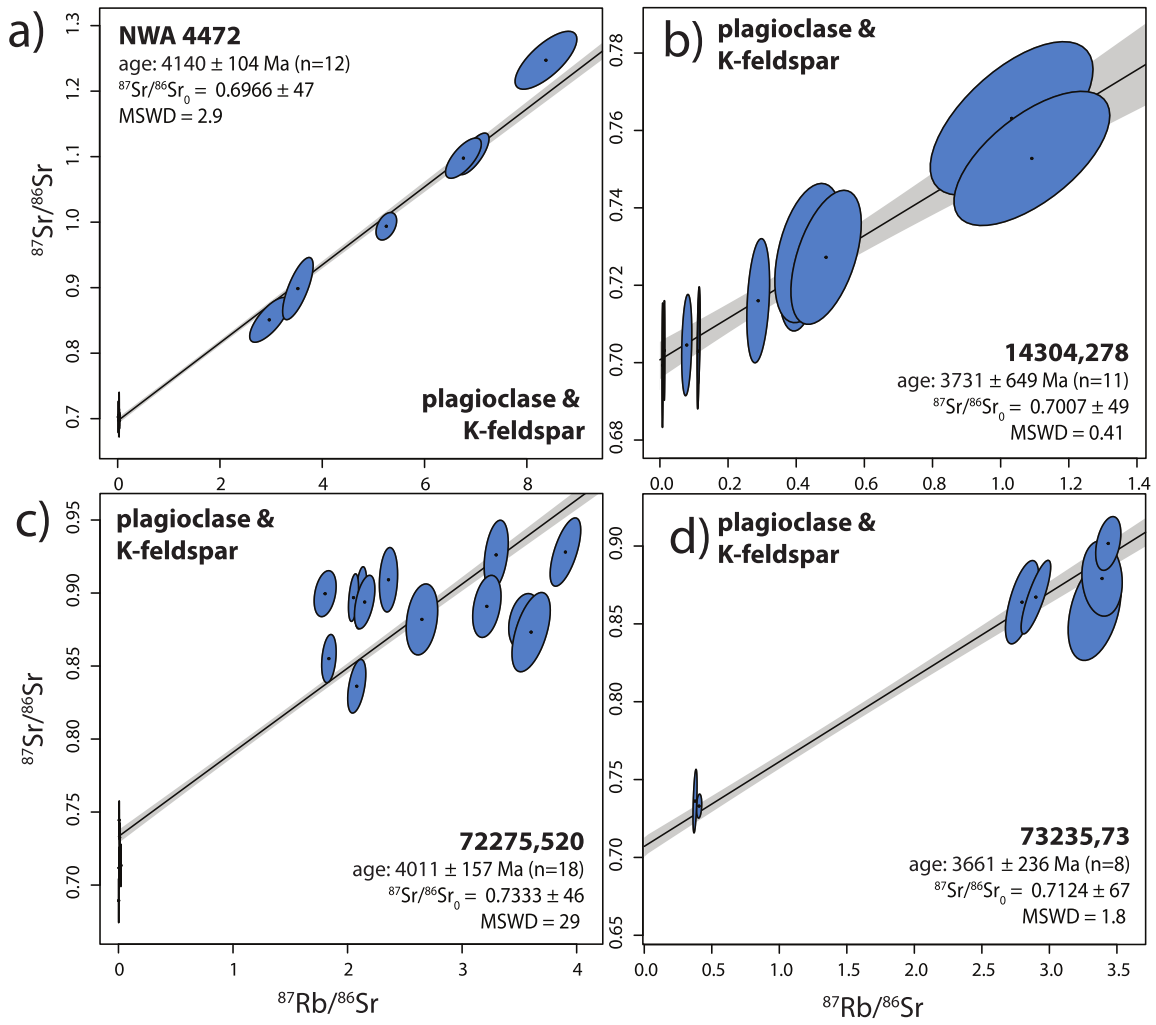

Figure 7. Plagioclase and K-feldspar $^{87}Sr/^{86}Sr$ vs. $^{87}Rb/^{86}Sr$ isochrons for samples NWA 4472, 14304,278, 72275,520 and 73253,73. Note that axis scales are different in each plot. Uncertainties are 2σ.

that the felsic area is interpreted to represent an impact melt, it may have incorporated Pb from other lithologies within the same sample.

3.5 U-Pb geochronology

Alkali gabbronorite clasts in samples 14304,278 and 14313,70 contain apatite sufficiently large to be targeted for U-Pb isotope analysis. These datasets are reported in Table S8 and summarised in Table 1. Following the gain corrections of the Pb isotopes and calibration of Pb-U ratios against the BR5 standard, the apatite U-Pb analyses were corrected for the presence of Pb not derived from the *in situ* decay of U in the apatites. Two alternative sources of such Pb were considered: (1) terrestrial contamination (e.g. modern terrestrial Pb as modelled by Stacey and Kramers, 1975); and (2) lunar initial Pb (as represented by the least radiogenic composition measured in the other Apollo 14 samples, from a feldspar in 14303,330). By performing two separate corrections, assuming 100 % of one or other of these sources, upper and lower estimates were obtained for the radiogenic isotope compositions of the apatites, both of which are reported in Table S8. When plotted in $^{207}Pb/^{206}Pb$ vs $^{204}Pb/^{206}Pb$ coordinate space (Fig. 12a, b), the uncorrected 14313,70 apatite analyses trend towards modern terrestrial Pb compositions and display little evidence of a contribution from lunar initial Pb (Fig. 12a). By contrast, the 14304,278 apatite analyses appear to trend towards the lunar initial Pb values indicated by the Pb isotope analyses of the other Apollo 14 and Apollo 17 samples, suggesting that the lunar initial Pb correction is more appropriate (Fig. 12a,b).

The four apatite analyses from 14313,70 yield a mean concordia intercept date of 3954 ± 15 Ma (MSWD = 240; Fig. 12c). However, three of these analyses are reverse discordant (7–38 %), likely due to the uneven surface of this sample mount. As has been discussed previously (Snape et al., 2016), Pb isotope ratios will be less affected by such analytical artefacts, therefore $^{207}Pb/^{206}Pb$ dates likely provide a more reliable age indication for such discordant analyses. The modern terrestrial Pb-corrected $^{207}Pb/^{206}Pb$ dates yield a weighted average of 3939 ± 11 Ma (MSWD = 0.18; p = 0.83; Fig. 12e). Due to variable and relatively high $^{204}Pb/^{206}Pb$ ratios in the sample (compared to typical apatites; e.g. those discussed below in 14304,278), a lunar initial Pb correction results in two younger $^{207}Pb/^{206}Pb$ dates with very large uncertainties (3155 ± 834 Ma and

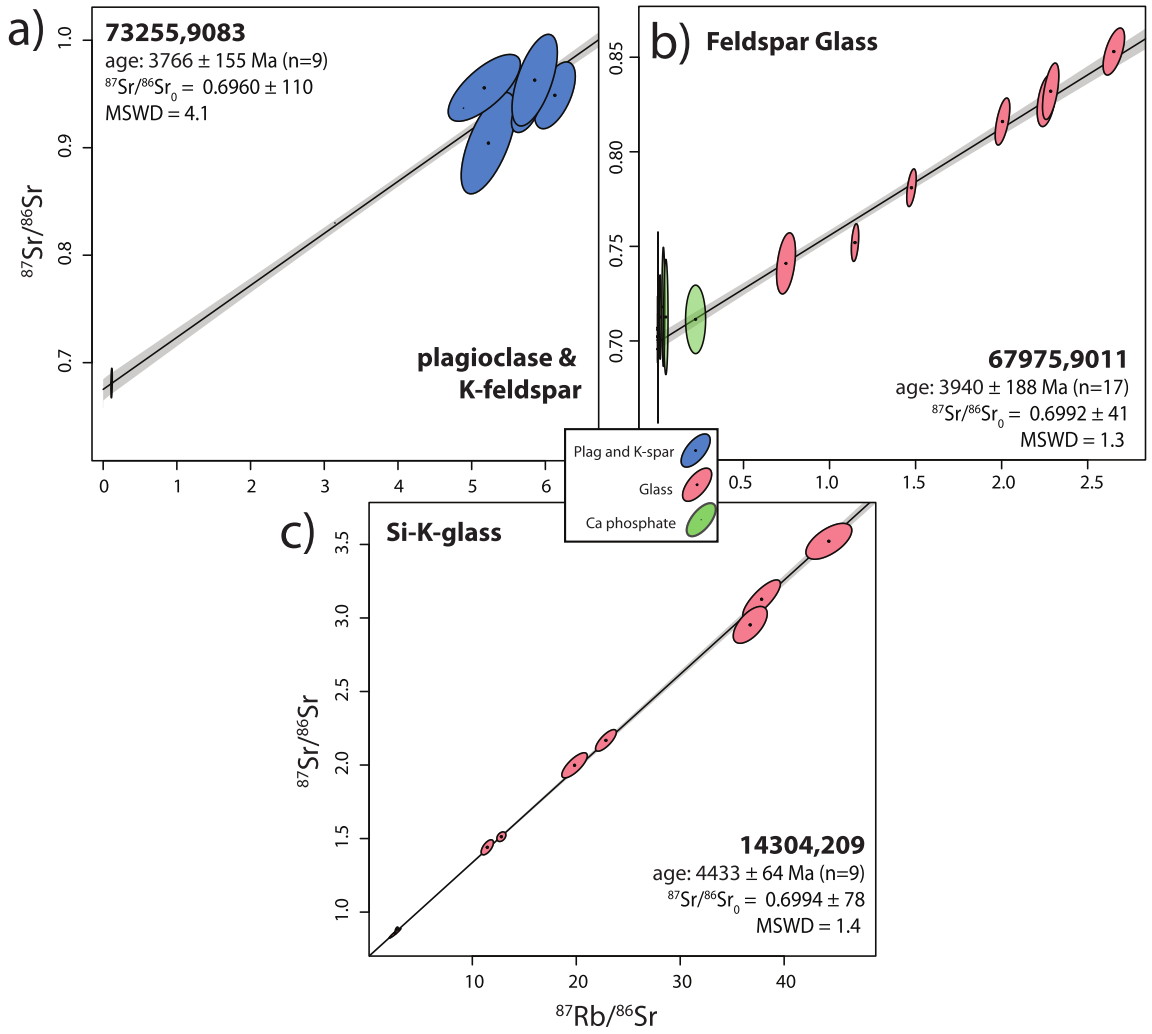

Figure 8. a) Plagioclase and K-feldspar $^{87}Sr/^{86}Sr$ vs. $^{87}Rb/^{86}Sr$ isochrons for sample 73255,9083. b) Feldspar glass (maskelynite) and Ca-phosphate $^{87}Sr/^{86}Sr$ vs. $^{87}Rb/^{86}Sr$ isochrons for sample 67975,9011. c) Si-K-rich glass $^{87}Sr/^{86}Sr$ vs. $^{87}Rb/^{86}Sr$ isochrons for sample 14304,209. Note that axis scales are different in each plot. Uncertainties are 2σ.

3106 ± 723 Ma; Fig. 12e), and a geologically implausible date (Fig. 12e). Taken together with the lack of evidence for a lunar initial Pb contribution, the modern terrestrial Pb-corrected dates $^{207}Pb/^{206}Pb$ (3939 ± 11 Ma) are considered to be more likely to be accurate.

Two apatite analyses from 14304,278 are slightly reverse discordant (7 % and 9 %). When corrected for modern terrestrial Pb, six concordant analyses from 14304,278 yield a concordia intercept date of 3921 ± 10 Ma (MSWD = 1.7; p = 0.11; green ellipses in Fig. 12d), whereas two analyses constrain an older intercept date of 4042 ± 92 Ma (MSWD = 1; p = 1; red ellipses in Fig. 12d). While this discrepancy may reflect varying degrees of resetting in the U-Pb system (see Section 4.3) it is notable that applying a lunar initial Pb correction pulls these two apparent age groups together. The lunar initial Pb corrected values for all ten analyses yield a weighted average $^{207}Pb/^{206}Pb$ date of 3915 ± 11 Ma (MSWD = 0.53; p = 0.85; Fig. 12f).

4 Discussion

Prior to assessing whether dates for the granitoid and alkali gabbronorite samples reported here (and in the literature) represent crystallisation ages, we must first assess the extent to which granitoids have been affected by secondary processes such as impact shock modification. This is critical, because such processes can act to modify the isotope system from which dates are calculated. It is only by using our best estimate of crystallisation ages, together with the geochemical constraints of mineral and bulk-rock chemistry, that we can assess the likely geologic setting that resulted in the formation of granitoids.

4.1 Evidence for shock modification

4.1.1 Feldspar Glass

The clasts investigated here display textural evidence of modification by shock-induced increase of temperature/pressure. Granitoid samples 73255,9083, 73255,9084, and alkali gabbronorite sample 67955,9011 contain glass with compositions indistinguishable from plagioclase/alkali feldspar (red open circles; Fig. 6). These glasses likely represent the

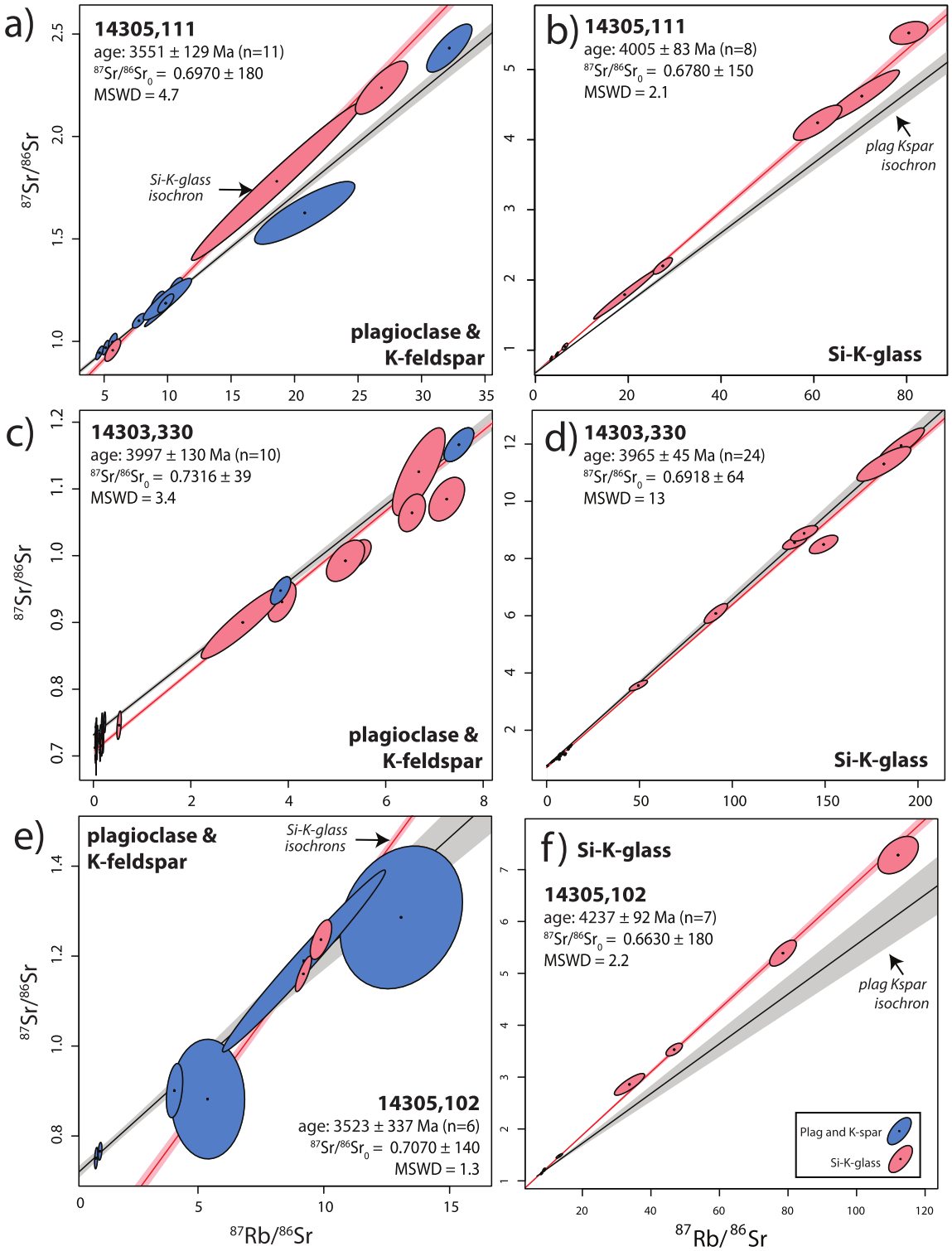

Figure 9. Rb-Sr isotopes for plagioclase and K-feldspar (blue symbols) and Si-K-rich glass (red symbols) for samples 14305,111, 14303,330, and 14305,102. The black line represents calculated plagioclase/K-feldspar isochron regression (and associated uncertainties, grey field), whereas the red line represents the calculated Si-K-rich glass isochron. Note that axis scales are different in each plot. Uncertainties are 2σ.

shock transformation of plagioclase/alkali feldspar to a glass phase. Shock pressure experiments indicate that plagioclase converts from crystalline to amorphous glass (i.e., maskelynite) at pressures of > 20 GPa (Stöffler et al., 1986; Bischoff and Stöffler, 1992; Fritz et al., 2017; Jaret et al., 2015). In the studied samples, the shock modification process that triggered crystal lattice transformation to glass appears to be very localised, as crystalline feldspar is also present within the same thin sections (Table S10). We note that maskelynite is defined as the shock transformation of feldspar without changes to chemistry or morphology (Binns, 1967). Therefore, these glasses are not maskelynite (or its alkali equivalent) *sensu stricto,* due to a small stoichiometric difference with crystalline feldspar (4.9 total cations per

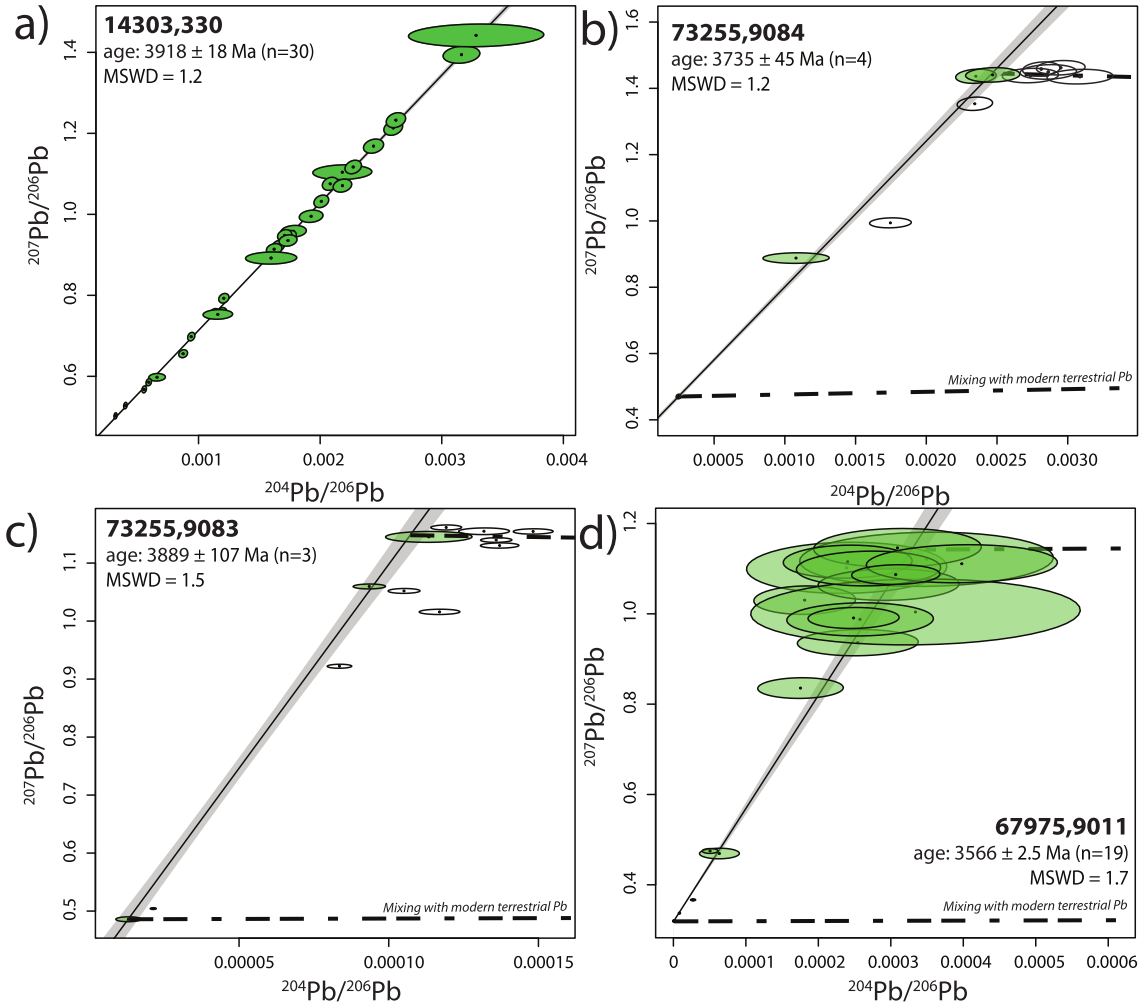

Figure 10. $^{207}Pb/^{206}Pb$ vs. $^{204}Pb/^{206}Pb$ analyses of plagioclase and K-feldspar from samples 14303,330, 73255,9084, 73255,9083, and 67975,9011. For b, c, and d, the assumed mixing relationship between the most radiogenic Pb, initial Pb, and modern terrestrial Pb (Stacey and Kramers, 1975) is illustrated by the dashed line. The vast majority of analyses fall close to the left-most edges of these triangles, defining the isochron for the samples (black line). White date points were excluded from the age calculation as they do not lie within the uncertainty of the left-most edge of the mixing triangle. Uncertainties are 2σ.

formula unit; Table S10). Such non-stoichiometric 'maskelynite' is commonly reported from Martian volcanic rocks where shock transformation of plagioclase is near-ubiquitous (e.g., Mittlefehldt, 1994; Scott et al., 1997; Greenwood and McSween, 2001) and has also been reported in other Apollo granitoids (Simon et al., 2020). The stoichiometric difference with feldspar reflects a total of 0.9 for the A-site cations (Na + K + Ca + Ba), despite their near 100 wt% oxide totals and T-site (Si + Al) cation totals of 4.0. Older plagioclase analyses with reported A-site deficiencies were argued to reflect Na loss during electron probe microanalysis (EPMA; e.g., Ruzicka, 1995). To mitigate this effect, a defocused EPMA beam is commonly employed. Although we cannot categorically rule out that the A-site deficiency reported here is an analytical artefact, the high temperatures associated with the generation of impact melts also make it difficult to exclude volatilisation of Na and K, during or following the formation of maskelynite, as the cause.

4.1.2 Ternary feldspar

Some feldspar compositions fall within the miscibility gap when plotted onto the feldspar ternary diagram (Fig. 4). While there is some evidence that increased Ba contents of feldspar will act to increase the stability field of feldspars (Morgan and London, 2003), the compositions reported here should not be thermodynamically stable at any pressure (Ghiorso, 1984). Erickson et al. (2024) demonstrated that similar ternary feldspars can have sub-microscopic (i.e., < 10 nm) textures consistent with spinodal decomposition (i.e., whereby a mineral phase spontaneously exsolves into two phases). Spinodal decomposition of alkali feldspar is common in terrestrial granites during slow cooling and results in greater than micron-scale perthitic textures (e.g., Petrishcheva et al., 2020). Some perthitic textures have been documented in Apollo 17 granitoids (Ryder et al., 1975) but are absent from the samples investigated here. Impact melting of plagioclase and alkali feldspar could result in a melt with a composition that falls within the feldspar

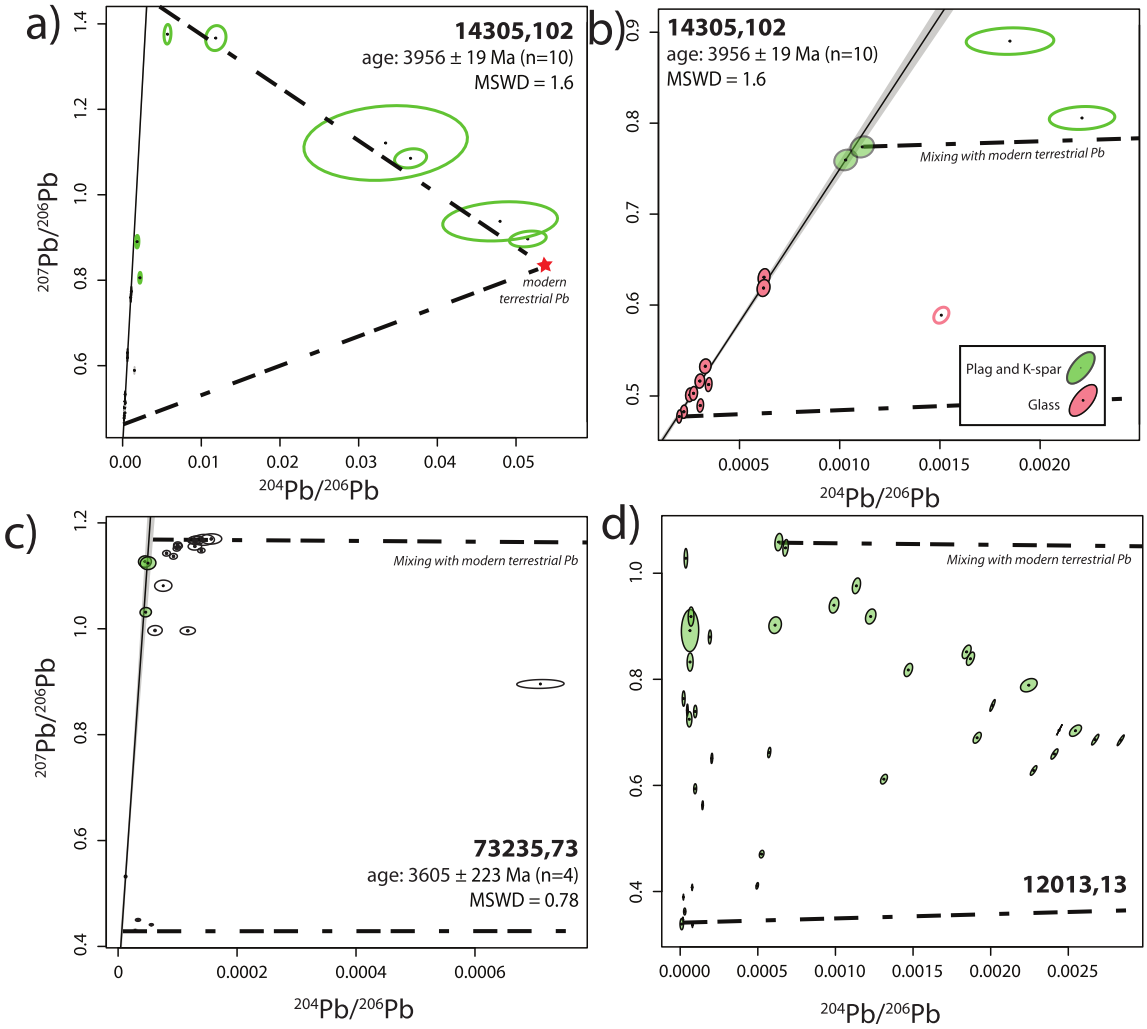

Figure 11. $^{207}Pb/^{206}Pb$ vs. $^{204}Pb/^{206}Pb$ analyses of plagioclase, K-feldspar and glass from samples 14305,102, 73235,73, and 12013,13. As with Fig. 10, the assumed mixing relationship between the most radiogenic Pb, initial Pb and modern terrestrial Pb (Stacey and Kramers, 1975) is illustrated by the dashed line. The vast majority of analyses fall close to the left-most edges of these triangles, defining the isochron for the samples (black line). White date points were excluded from the age calculation as they do not lie within the uncertainty of the left-most edge of the mixing triangle. Uncertainties are 2σ.

miscibility gap; if such a melt then experienced undercooling, this would act to preserve this metastable composition (Erickson et al., 2024). It is unclear if this process is linked to shock; however, given the occurrence of Si-K-rich impact glass (see below), this is the most likely explanation.

4.1.3 Si-K-rich glass

Si-K-rich glass regions within these samples have higher K abundances than Apollo granitoid bulk rock compositions (Fig. 6a). Rather, the Si-K-rich glass is more similar to the range of compositions found within mare basalt and KREEP basalt mesostasis regions (Fig. 6). Mesostasis represents the residual liquid during the final few percent crystallisation of a basaltic liquid, normally occurring as small (< 100 µm) regions between the main rock-forming minerals (Potts et al., 2016; Pernet-Fisher et al., 2014). However, the Si-K-rich glass observed here is not texturally consistent with mare basalts mesostasis (see textural description of Si-K-rich glass in Section 2).

The occurrence of Si-K-rich glass in granitoids has been interpreted to represent impact melt derived from melting precursor felsic rocks (Ryder et al., 1975; Shervais and McGee, 1999; Grange et al., 2009; Barboni et al., 2025). Rock types such as granites have the lowest melting point of any silicate igneous rock, making them susceptible to shock-induced melting (Shervais and Taylor, 1983); in hydrous systems, granites start to melt at < 800 °C (Holtz and Johannes, 1991; Lamadrid et al., 2014), and in anhydrous systems, granites start to melt from ~950 to 1000 °C (e.g., Newton, 1986; Liaw et al., 2006). The lack of significant native Fe within these glasses, and their low abundance of siderophile elements such as Co or Ni relative to impact melts (Si-K-rich glass have Ni < 85 µg g^{-1}, Table S11, vs. > 200 µg g^{-1} in clast-rich and clast-poor impact melts; Papike et al., 1998), indicate that these glasses are not part of large-scale impact melt ejecta or melt sheet complexes (e.g., poikilitic impact melt breccias; Ryder and Spudis, 1987; Norman et al., 2002), but more likely represent localised

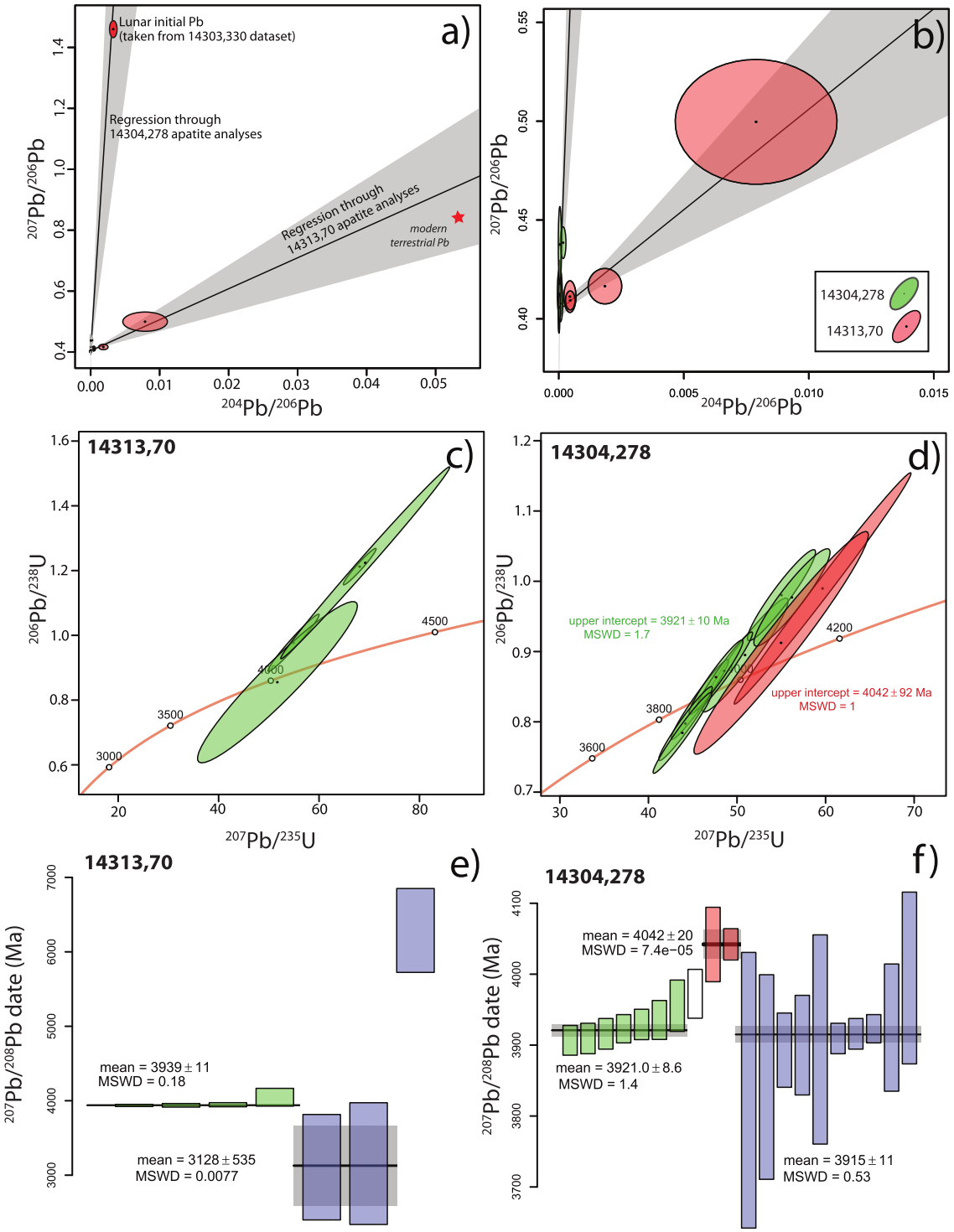

Figure 12. a) and b) Phosphate analyss from samples 14313,70 (green ellipse) and 14304,278 (red ellipse) plotted in $^{207}Pb/^{204}Pb$ vs. $^{204}Pb/^{206}Pb$ space. Regression through analyses for 14131,70 trend towards modern terrestrial Pb whereas a regression through analyses for 14304,278 trend towards lunar initial Pb values. Modern terrestrial lead corrected $^{206}Pb/^{238}U$ versus $^{207}Pb/^{235}U$ concordia plots are also presented for 14313,70 (c) and 14304,278 (d). e) and f) report $^{207}Pb/^{206}Pb$ dates for 14313,70 and 14304,278 respectively. Terrestrial corrected ages are plotted in green and red and the lunar initial corrected values are plotted in blue. Modern terrestrial Pb isotope ratio in a) is from Stacey and Kramers (1975). All errors are 2σ.

impact-induced melting (i.e., melt formed by conductive heat transfer alone and not linked to an increase in pressure). The preservation of Si-K-rich glass in granitoids 14305,111, 14305,102, 14303,330, and 14304,209 (Fig. 1), thus, likely reflects very rapid quenching of a melt(s). Glass in sample 12013,13 may reflect formation from a slower-cooling melt relative to the other glass-bearing samples, allowing both silica and K-feldspar to crystallise as distinct mineral phases (Fig. 1j,k). The Si-K-rich glass within alkali gabbronorite sample 67975,9011 could represent a melt mesostasis:

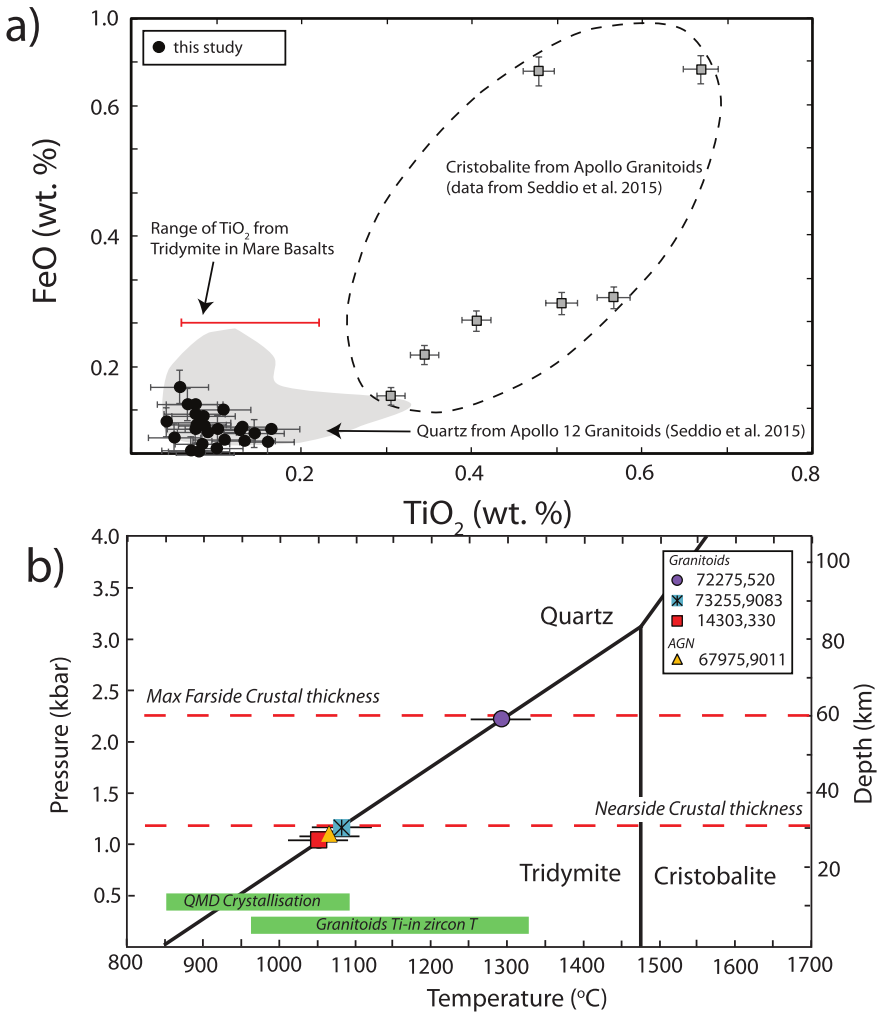

Figure 13. a) FeO vs. TiO_2 wt% for silica polymorphs from Apollo granitoids. Black symbols are from the samples in this study, grey symbols and field are from Seddio et al. (2015). The red bar represents the range of TiO_2 reported from tridymite in mare basalts (Smith and Steele, 1984). We note that the range of TiO_2 in granitoid quartz grains overlaps the range of TiO_2 of tridymite. b) Low-pressure field of the SiO_2 phase diagram (Tuttle and Bowen, 1958). Temperature estimates using the Ti-in-K-feldspar are plotted along the quartz/tridymite transition to estimate the lowest possible crystallisation pressure. For reference, near- and farside crustal thicknesses are plotted (red dashed lines). Green bars indicate estimated crystallisation temperature of quartz monzodiorites (Barrett et al., 2023) and granitoids using Ti-in-zircon (Crow et al., 2017).

texturally, the glass is present in small regions between pyroxene and plagioclase. However, significant Si-K-rich glass is also present surrounding mineral grains and filling cracks. This could indicate some infiltration or remelting and redistribution of felsic melts throughout the sample, possibly as an impact melt.

4.2 Temperature-pressure estimates

Pressure and temperature constraints can help refine models of melt generation, evolution and crystallisation. However, the precise petrogenesis of lunar evolved melts is poorly constrained, and very few pressure-temperature (P-T) estimates have been reported (Seddio et al., 2015; Shearer et al., 2022). Previous studies have estimated crystallisation depths to first order by identifying which silica polymorphs are present. The occurrence of high-temperature silica polymorphs tridymite (870–1470 °C) and cristobalite (1470–1705 °C; Wenk and Bulakh, 2016) has been used to argue that granitoids represent shallow magmatism (within the top few km of the lunar crust), possibly analogous to siliceous domes such as those seen at the lunar nearside Gruithuisen region (Seddio et al., 2015; Shearer et al., 2022). However, as noted by Barrett et al. (2023), at temperatures > 1050 °C, tridymite is a stable crystallising silica phase throughout the crust (i.e., down to ~30 km depth on the lunar nearside).

To perform more quantitative pressure/temperature estimates, there are limited options for lunar granitoids due to the mineral phases present (e.g., there is an absence of pyroxene, which is commonly used to estimate P-T conditions). Recently, a method for calculating crystallisation temperatures using Ti-in-K-feldspar has been established for felsic magmatic systems (Zhang et al., 2022). It is important to note that this system has been calibrated for terrestrial systems over a limited range of temperatures (500 to 800 °C) and pressures (2 to 3 kbar), and for Ti abundances up to ~150 μg g^{-1}. When applied to the K-

feldspars investigated here (using Ti abundances determined by LA-ICP-MS; Table S11), we obtain results that appear reasonable for depths across the Moon's crustal structure. Only four of the samples contain K-feldspar grains that are large enough to determine their trace element systematics (granitoids 72275,520; 73255,9083, 14303,330 and alkali gabbronorite 67975,9011). The Ti abundances measured for each sample (778 ± 26, 313 ± 50, 349 ± 25, and 333 ± 24 μg g^{-1}, respectively; uncertainties 2SE) correspond to calculated temperatures of 1293, 1054, 1078, and 1067 °C (note the model calibration has a standard error estimate of ±70 °C, which is larger than the propagated analytical uncertainties). The temperature-pressure relationship during shock metamorphism is well established (e.g., Stöffler and Langenhorst, 1994). If the temperatures calculated here were to record peak metamorphic temperatures rather than crystallisation temperatures, the expected corresponding peak metamorphic pressures should exceed 500 kbar. Under these pressure and temperature conditions, the silica polymorph coesite should be present within these samples, but it is not observed.

The range of temperatures reported here (1054 to 1293 °C) is consistent with those calculated using Ti-in-zircon thermometry from multiple thin sections of Apollo 15 sample 15405 (958 to 1321 °C; Fig. 13b Valley et al., 2013; Crow et al., 2017). The lower bound of this range is consistent with the dry solidus for granites (e.g., Robertson and Wyllie, 1971). Except for sample 72275,520, our calculated temperatures are also within the range of crystallisation temperatures reported for quartz monzodiorite samples (Barrett et al., 2023; First and Rutherford, 2019, Fig. 13b).

Titanium-in-quartz is frequently used as a thermobarometer for evolved terrestrial magmas (e.g., Wark and Watson, 2006; Thomas et al., 2010). Despite this, as discussed by Seddio et al. (2015) and Barrett et al. (2023), this system may not be suitable for application to silica in lunar granitoids. As a first-order limitation, this system requires an independent temperature estimate in order to calculate a pressure (and *vice versa*). Additionally, whereas quartz has been identified as the stable silica polymorph in the granitoids investigated here (Fig. S11), it has been argued that silica grains from lunar granitoids have undergone a volumetric contraction caused by the transition from less-dense cristobalite or tridymite to more-dense quartz (Seddio et al., 2015). Both tridymite and cristobalite can incorporate more Ti in their crystal structure for a given P-T relative to quartz due to their relatively open crystal structures (Smith and Steele, 1984). Consequently, quartz that originated as a higher-T polymorph may display higher Ti abundances than quartz that crystallised directly from a melt. Indeed, Seddio et al. (2015) noted that the range of Ti content reported for silica in Apollo 12 granitoid clasts (grey field in Fig. 13a), and by extension the range of Ti content in silica observed in our study (black symbols in Fig. 13a) are within range of tridymite found in mare basalts (red line in Fig. 13a). Consequently, any calculated pressures or temperatures will be spurious using either our specific Ti-in-quartz routine (Table S13) or the less precise defocused beam routine used for all felsic phases (Table S10). Indeed, using the Ti-in-K-feldspar temperatures, the resulting Ti-in-quartz pressures yield values that range from 9 to 22 kbar. For the Moon, these pressures correspond to depths > 100 km (i.e., within the lunar mantle) and clearly do not represent granitoid or alkali gabbronorite crystallisation depths.

In the absence of a reliable barometer, it is not possible to constrain meaningful crystallisation pressure estimates for the granitoids and alkali gabbronorites studied here. However, the maximum possible crystallisation pressure can be estimated using the point at which tridymite is no longer stable within the lunar crust (assuming that the quartz observed here originally crystallised as tridymite). On this basis, the granitoids we have data for could have crystallised at any depth within the nearside lunar crust (Fig. 13b).

4.3 Interpreting granitoid and alkali gabbronorite dates

Dates reported here, together with those reported in the literature, are plotted in Figures 7 to 12 and Figure 14. All uncertainties cited here are at the 2σ level.

U-Pb and Pb-Pb isotope dates

The Pb-Pb isotope data reported here significantly expand the number of Pb-Pb isotope analyses available for lunar granitoids and alkali gabbronorites across multiple Apollo landing sites. Previously, Nemchin et al. (2017, 2021) highlighted that the Imbrium impact event at 3922 ± 12 Ma must have 'profoundly' homogenised Pb between minerals in granitoids excavated from depth by the basin-forming event, and in the impact breccias that were formed during the event. While acknowledging the complications in determining ages from samples reported here (see Section 3.4), at face value, Si-K-rich glass dates for samples 73255,9083, 14303,330 and 14305,105 are within uncertainty of the age of Imbrium (Fig. 14a). Notably, our Pb-Pb date for 14303,330 (3918 ± 18 Ma) is within uncertainty of the 3920 ± 13 Ma date reported by Nemchin et al. (2017) for K-feldspar within a different granitoid clast within sample 14303,49. Granitoids 73235,73 and 73255,9084, and alkali gabbronorite 67975,9011 have dates that are younger than Imbrium. At face value, these dates could represent Pb isotope resetting/partial resetting by younger impact events (Fig. 14a). These ages are consistent with reported bulk-rock Ar-Ar dates (ranging from 3.88 to 3.69 Ga for samples 14305, 14303, 14304, 14313, 67975, 73235, 73255, 72273; Kirsten et al., 1972; Phinney et al., 1975; Turner and Cadogan, 1975; Jessberger et al., 1978), indicating that impacts such as Imbrium or younger were responsible for the assembly of the host breccias in which the granitoids are situated.

There are very few U-Pb Ca-phosphate dates previously reported for Apollo and lunar meteorite granitoid samples – dates range from 3911 ± 42 to 3959 ± 35 Ma for 12013,7 (Thiessen et al., 2018) and from ~3.94 to ~4.15 Ga for the Calcalong Creek meteorite (Oliveira et al., 2025) – and none are reported for alkali gabbronorite samples. We obtained Ca-phosphate dates of 3915 ± 11 Ma from 14313,70 and

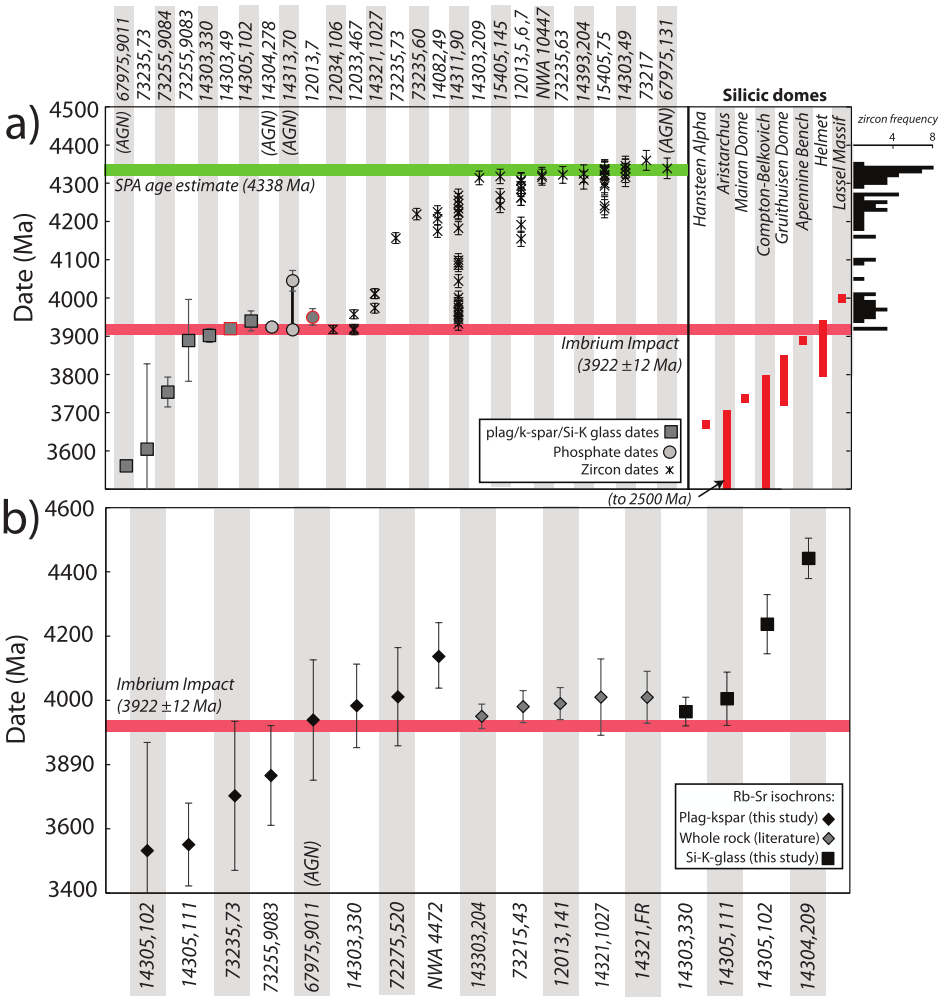

Figure 14. a) U-Pb, Pb-Pb, and b) Rb-Sr isotope dates of granitoid material reported here and summarised from the literature. Pb-Pb and U-Pb dates from this study have red outlines. Literature Pb-Pb data from Nemchin et al. (2017). Ca-phosphate U-Pb data from Thiessen et al. (2018). Zircon literature data from Compston et al. (1984); Meyer et al. (1989); Thiessen et al. (2018); Meyer et al. (1996); Crow et al. (2017); Nemchin et al. (2008); Grange et al. (2013); Zeng et al. (2021). For sample 73217, Compston et al. (1984) did not report the sub-split number analysed. Literature whole-rock Rb-Sr dates from Albee et al. (1970); Compston et al. (1977); Shih et al. (1985); Shih et al. (1994); Simon et al. (2011). Impact crater counting absolute model ages of silicic domes are plotted as red bars; data from Shearer et al. (2023) and references therein. Imbrium basin impact age from Nemchin et al. (2021). The yellow bar represents our best estimate for the crystallisation age of lunar granitoids (uncertainty is 2σ). The upper South Pole-Aitken basin age estimate is from Barboni et al. (2024).

3939 ± 25 Ma for 14304,278 (Fig. 10). It is evident that the U-Pb isotope system of Ca-phosphates within alkali gabbronorite samples (and granitoids based on published dates) has been reset by the Imbrium impact event (Fig. 14a). This is also consistent with the susceptibility of Ca-phosphates to shock pressure damage by impacts (e.g., Černok et al., 2019).

In contrast to Ca-phosphates, many granitoid clasts from 16 Apollo samples have zircon $^{207}Pb/^{206}Pb$ dates reported (99 analyses across 69 zircon grains; Compston et al., 1984; Meyer et al., 1989, 1996; Nemchin et al., 2008; Crow et al., 2017; Grange et al., 2013; Trail et al., 2020; Zeng et al., 2020). The frequency distribution of reported zircon $^{207}Pb/^{206}Pb$ dates are plotted on the right-hand side of Figure 14a. To avoid over-sampling, in the cases where multiple analyses were made on a single zircon grain, we plotted the oldest date on the basis that this likely reflects the least impact-modified age. Zircon dates yield clusters between 3.92 and 4.01 Ga, ~4.16 to 4.27 Ga, and ~4.29 to 4.35 Ga (Fig. 14a).

In general, zircon grains present in igneous clasts largely survive heating and abrasion associated with impact and breccia formation (e.g., Nemchin et al., 2008). This argument is used to suggest that the oldest dates recorded by zircons reflect the age of magmatic events (e.g., Kring et al., 2015; Barboni et al., 2024). A weighted mean of the oldest cluster of zircon dates (across 27 zircon analyses) yields a date of 4320 ± 2 Ma. The significance of this date within the lunar zircon population has recently been discussed by Kring et al. (2015) and Barboni et al. (2024) and is further discussed in Section 4.4.

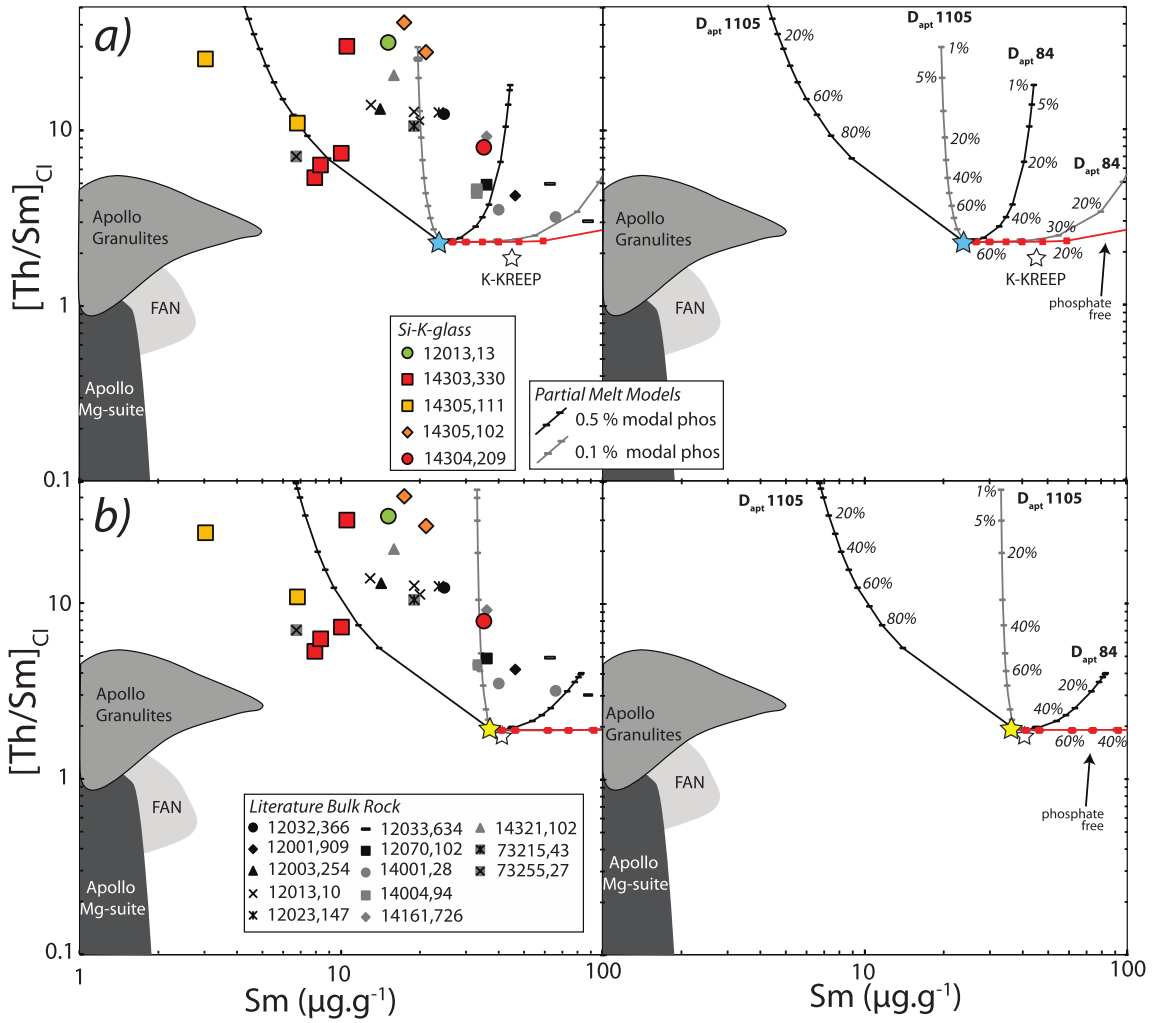

Figure 15. Plots of $[Th/Sm]_{CI}$ vs. Sm for lunar highland lithologies. Apollo granulites, Mg-suite, and FAN data from Lindstrom and Lindstrom (1986), Papike et al. (1998) and Papike et al. (1997). Literature bulk rock data for Apollo granitoids are from Meyer (2011), Warren et al. (1983) and Warren et al. (1987). High-K KREEP from Warren (1989). Red lines represent Ca-phosphate-free partial melting; black and grey lines represent partial melting with 0.5 and 0.1 modal % Ca-phosphate in the source lithology, respectively. Blue star in a) represents the melting of a Si-rich lithology, whereas the yellow star in b) represents the melting of an Fe-rich lithology. See Supplementary Materials for details of the partial melting calculations.

It is unclear whether zircon dates < 4.32 Ga reflect impact resetting/partial resetting or crystallisation ages. Some samples (such as 12013,5, 12013,6, 12013,7 and 14303,49) have relatively large numbers of zircon analyses (n = 8 for 12013 and 15 for 14303,49 respectively) that display a spread of dates. For these samples, dates range from 4154 to 4308 Ma for 12013,5,6,7 and from 4228 to 4346 Ma for 14303,49. Partial resetting of the U-Pb system due to Pb loss is argued to be the cause of the spread from ~4.3 Ga to younger dates in these samples (Nemchin et al., 2008; Grange et al., 2013; Thiessen et al., 2018; Barboni et al., 2025). Impact-related shock is known to result in distinct microstructural and textual characteristics in zircons (e.g., Timms et al., 2011; Crow et al., 2017, 2019). However, for the most part, such observations are absent. Additionally, for many samples, only several zircon grains were available for analysis, many of which plot along the condordia curve in U-Pb isotope space (Meyer et al., 1996). While the age of the youngest zircons (~3.92 Ga) is likely related to the Imbrium impact event, it is difficult to robustly assess whether < 4.32 Ga dates reflect an impact-reset age or a (re)crystallisation age. Irrespective of this, it is evident from the zircon population that lunar granitoids are older than ~ 3.92 Ga; i.e., formed before the Imbrium impact event (Fig. 14a).

Rb-Sr isotope dates

Figure 14b shows our plagioclase, alkali feldspar, and Si-K-rich glass isochron dates together with reported whole-rock Rb-Sr dates. All uncertainties cited here are at the 2σ level. Our dates for 14303,330 (both plagioclase and K-feldspar (3997 ± 130 Ma) and Si-K-rich glass (3965 ± 45 Ma) isochron dates) are within the uncertainty of the reported whole-rock date of 3950 ± 38 Ma (14303,204; Shih et al., 1994).

Although the Rb-Sr chronometer is typically resistant to impact shock effects < 10 GPa, it can be significantly affected by subsequent thermal annealing, resulting in partial or complete re-equilibration of the Rb-Sr system (e.g., Borg et al., 2005; Schärer and Deutsch, 1990; Gaffney et al., 2011). At temperatures around 700 to 1000 °C, Sr and Rb have similar diffusion rates in both plagioclase and alkali feldspars, both moving 100s of microns over decades (Giletti, 1991). All Apollo plagioclase and K-feldspar isochron dates reported here, together with reported whole-rock Rb-Sr dates, are within range of the Imbrium impact event at 3.92 Ga or younger (Fig. 14b); this indicates that the Rb-Sr chronometer has likely been partially to totally reset by lunar nearside impact events.

Lunar meteorite sample NWA 4472 has a plagioclase/K-feldspar date of 4140 ± 140 Ma. On the basis that granitoid fragments within this sample also contain Si-K-rich glass, it is likely that this date also represents an impact reset/partial reset age rather than a crystallisation age. Phosphates from other clasts and the matrix of this sample have U-Pb dates that range from 4344 ± 14 to 3931 ± 18 Ma (Joy et al., 2011), indicating that our Rb-Sr date is likely a partially reset age from an older (~4.34 Ga) granitoid crystallisation age. We note that U-Pb analyses of Ca-phosphates from Apollo 17 samples record a distinct reset event at ~4.2 Ga, which has been tentatively linked to the formation of the Serenitatis impact basin (Černok et al., 2021). Therefore, we cannot rule out that the Rb-Sr isotope systematics in granitoid fragments 14305,102 are preserving the Serenitatis impact event rather than reflecting partial resetting by the Imbrium basin-forming event.

As noted in Section 3.3, Rb-Sr isochron dates calculated using analyses from Si-K-rich glass have calculated $^{87}Sr/^{86}Sr_0$ initial values below the Sr isotope growth curve from the lunar initial (Figs 8, 9); and samples 14305,111 and 14305,102 have Si-K-rich glass Rb-Sr isochron dates that are older than plagioclase/K-feldspar isochron dates (Fig. 9 and Fig. 14b). It is notable that Si-K-rich glass isochrons have $^{87}Rb/^{86}Sr$ values > 3. The spuriously low Sr isotope initial values could, thus, be a computational artefact as there are few datapoints with $^{87}Rb/^{86}Sr$ values close to zero to help robustly constrain the regression intercept. However, this could also reflect preferential Rb loss relative to Sr from the Si-K-rich glass. Variable Rb loss from different glass patches could lower $^{87}Rb/^{86}Sr$ ratios, resulting in steeper isochrons that regress to low initial Sr isotope ratios and yield spuriously old dates. This effect could also account for the old date (4433 ± 64 Ma) yielded by glass analyses from 14304,209, even though its calculated $^{87}Sr/^{86}Sr_0$ initial value is above the Sr isotope growth curve from the lunar initial. The loss of Rb and other volatile elements (e.g., Pb, K, Na) relative to refractory elements during impact vaporisation is commonly reported from Apollo and Chang'e 5 impact glasses (Delano et al., 1982; Korotev et al., 2010; Yang et al., 2022). Indeed, Rb is one of the low-temperature group of moderately volatile elements (elements that have a 50 % condensation temperature <1300 K; Lodders, 2003; Albarède, 2009). Sossi et al. (2019) reported that Rb has a 1 % evaporation temperature of 1668 K (1395 °C), whereas K has a 1 % evaporation temperature of ~1867 K (1594 °C). It is not clear if the Si-K-rich glass has undergone K loss relative to refractory elements; therefore, this brackets the maximum temperature for Rb loss to have occurred. Experimental volatilisation experiments under lunar conditions by Gibson Jr et al. (1973) indicate that significant Rb loss from basaltic glass can occur at temperatures as low as ~1100 °C, setting a lower temperature estimate for Rb loss. The effect of impact-related Rb loss disturbing Rb-Sr isochrons has recently also been highlighted by Li et al. (2023), where significant loss of Rb is evident in analyses of mesostasis pockets from Chang'e 5 basalts; these analyses have high Sr isotope ratios (> 0.77), indicating long-term radiogenic growth of ^{87}Sr, yet have very low $^{87}Rb/^{86}Sr$ values (< 0.3) suggesting recent Rb loss. Together, this indicates that shock-related disturbance tends to lower $^{87}Rb/^{86}Sr$ ratios due to Rb loss, producing steeper isochrons and thus yielding older meaningless dates. Therefore, we suggest that caution should be used when interpreting the Rb-Sr isotope systematics of impact glass.

4.4 Assessing the geologic formation setting of granitoids

The basaltic underplating model was first advocated for in a lunar context by Hagerty et al. (2006) as a mechanism for generating large volumes of melt needed to account for the silicic magmatic domes identified at the lunar surface. The majority of zircon dates calculated using the U-Pb isotope system are older than the model impact crater counting ages for silica domes (~3.6 to ~4 Ga; Fig. 14). Therefore, it is not evident to us that mechanisms for generating large volumes of silicic melt (i.e., underplating) are necessarily needed to account for the occurrence of (at least some) lunar granitoids. Indeed, given the small size of granitoid fragments within the Apollo collection, it is not possible to estimate the size of the parent rocks from which the samples were sourced. The granitoids investigated here could have equally originated from granophyre horizons from within plutonic intrusions and/or differentiated impact melt sheets. In terrestrial settings, granophyre horizons are commonly observed in layered intrusions (e.g., Skaergaard; Hirschmann, 1992) and differentiated impact melt sheets (e.g., Sudbury; Keays and Lightfoot, 2020). Based on the available age information summarised above, it is not possible to differentiate between these two geological settings (i.e., mantle partial melts vs. impact-related crustal melting).

Impact melt sheets

The oldest cluster of zircon dates at ~4.32 Ga is notably older than current estimates for the largest nearside basins (Serenitatis, Crisium, Nectaris and Imbrium; Fassett et al., 2012). Thus, it is unlikely that differentiated impact melt sheets in any of these younger impact basins were the geological setting for the formation of granitoids. However, formation in differentiated melt sheets in the largest and oldest lunar impact basins cannot be ruled out. The oldest visible basin is the farside South Pole-Aitken basin (SPA).

Its age is actively debated (Fig. 14); estimates range from ~4.25 Ga, as possibly recorded by samples returned from the farside Apollo basin by Chang'e 6 (Su et al., 2025), to ~4.34 Ga, as recorded by zircon dates from a range of Apollo and meteorite samples (Kring et al., 2015; Barboni et al., 2024; Joy et al., 2024). Notably, the older age is consistent with an estimated minimum age of ~4.3 Ga inferred from a re-examination of impact crater counts using GRAIL data (Evans et al., 2018). Potentially even older is the postulated nearside Procellarum impact basin (Wilhelms et al., 1987), although it is debated whether this feature represents an impact basin or not (e.g., Cadogan, 1974; Andrews-Hanna et al., 2014; Whitaker, 1981).

Plutonic layered intrusions

A date of ~4.35 Ga marks the start of a period of secondary crust formation by plutonic magmatism recorded by the Apollo Mg-suite and High Alkali Suite lithologies (e.g., Borg and Carlson, 2023). The causes for the generation of mantle partial melts at this time range from a mantle overturn event – driven by instabilities of dense ilmenite-bearing layers at the top of the magma ocean cumulate pile or triggered by the SPA impact (Kring et al., 2015; Borg and Carlson, 2023; Prissel et al., 2023; Barboni et al., 2024) – to a period of tidal heating (Nimmo et al., 2024). Regardless of the causes of magmatism, the range of zircon dates within the ~4.32 to 4.34 Ga cluster could reflect their crystallisation within magmatic intrusions emplaced in the crust at the end of this magmatic period.

4.5 Assessing the chemistry of potential parental melts

At face value, low reported bulk-rock and mineral/glass siderophile element abundances (Papike et al., 1998) together with a lack of phases such as native Fe within granitoids, would seem to preclude their origin within an impact melt sheet. This is further indicated by the bulk rock and Si-K-rich glass trace element systematics. As highlighted previously, reported granitoid bulk rock analyses and Si-K-rich glasses are enriched in incompatible trace elements. Whereas absolute REE abundances are within range of Apollo high-K KREEP (Fig. 3), incompatible element ratios display a notable difference, e.g., higher Th/Sm than high-K KREEP (Fig. 15). Such ratios (assuming the chemistry of the impact-generated Si-K-rich glass reflects the bulk composition of the precursor granitoids) are unlikely to reflect a parental melt formed by impact-generated crustal melting. Impact melts may be superheated to temperatures far above the normal melting point of silicate rocks (e.g., Bray et al., 2010). This would result in nearly 100 % melting of the target crust, forming an impact melt 'pond' that then undergoes differentiation. Such high degrees of melting would not fractionate incompatible trace elements; rather, the trace element abundances would reflect those of the melted crustal lithologies. Therefore, the fact that granitoid Th/Sm ratios cannot be accounted for by any mix of known highland lithologies and KREEP might indicate a different magmatic origin, either in mantle source contributions or melting regime, relative to other highland lithologies (Korotev et al., 2003; Pernet-Fisher et al., 2024).

Some have argued that lunar granitoids are the result of large-scale silicate liquid immiscibility (SLI; Quick et al., 1977; Neal and Taylor, 1989; Jolliff et al., 1991). During the crystallisation of magmatic systems, in the final few percent of solidification, the residual liquid can enter an immiscibility field where it will separate into Si-rich and Fe-rich fractions. The REEs and P would preferentially partition into the latter, and K would preferentially partition into the former. Silicate liquid immiscibility is commonly observed in mare basalts (Potts et al., 2016; Zhang et al., 2025; Pernet-Fisher et al., 2014; Roedder and Weiblen, 1970) and has been experimentally reproduced for lunar mare basaltic systems and lunar magma ocean crystallisation (Hess et al., 1975; Rutherford et al., 1976; Zhang et al., 2024; Ofierska et al., 2026). Lunar granitoids have bulk-rock K/REE and K/P ratios consistent with the expected composition of the Si-rich immiscible fraction; however, the range of Th/Sm values observed is not consistent with the expected Si-rich fraction (Watson, 1976; Warren et al., 1983). Partition coefficients between immiscible Fe-rich and Si-rich melts for basaltic systems suggest that REEs and Th have similar partitioning behaviour ($D_{Fe\text{-}liq/Si\text{-}liq}$ = 2.01 ± 0.73 for Sm and 1.59 ± 0.54 for Th; Veksler et al., 2006). Therefore, during the separation of immiscible melts, the Th/Sm value should not fractionate significantly. Rather, the fractionation of incompatible element ratios like Th/Sm to higher values than high-K KREEP has been argued to reflect either the crystallisation of Ca-phosphates in the granitoid parent melt prior to SLI (Neal and Taylor, 1989) or Ca-phosphates contributing to partial melts of either a precursor Si-rich lithology (Zhang et al., 2024) or a fertile mafic crust, i.e., basaltic underplating (Hagerty et al., 2006).

Crystallisation of Ca-phosphates, and merrillite in particular, are one of the key mineral groups (together with zircon) for constraining the incompatible trace element budget of granitoids (Seddio et al., 2015). This is due to the high abundance of incompatible elements, such as the REEs, in Ca-phosphates relative to silicate minerals. There are few constraints on mineral/melt partition coefficients for Ca-phosphates in evolved terrestrial or lunar magmatic systems. Merrillite/melt and apatite/melt partition coefficients compiled from the GERM database and those reported by Neal and Taylor (1989) indicate that Ca-phosphates have REE partition coefficients 10 to 100 times higher than Th. Thus, melt Th/Sm values should be significantly fractionated during partial melting and/or fractional crystallisation of Ca-phosphate-bearing assemblages. Due to a lack of robust constraints on mineral/melt partition coefficients for evolved lunar systems, it is difficult to precisely quantify the role that Ca-phosphates play in fractionating trace elements. Using terrestrial partition coefficients for evolved systems (see Table S14 in Supplementary Materials for values used), we illustrate the potential for Th/Sm fractionation in partial melts from Ca-phosphate-bearing and Ca-phosphate-free Si-rich and fertile mafic starting compositions (Fig. 15).

Si-rich parental melt

Zhang et al. (2024) demonstrated that urKREEP (the KREEP-rich residue of lunar magma ocean crystallisation situated between the crust and mantle) will have undergone SLI and argued that a partial melt from the crystallised product of the Si-rich fraction (a lithology that would likely be similar to granitoids) could play a role in the genesis of lunar granitoids. It is hard to estimate the incompatible element abundances in the Si-rich fraction of urKREEP. Partitioning data suggest that around half to a quarter of the REE and Th budget should partition into the Si-rich fraction relative to the Fe-rich fraction; REEs have reported $D_{Fe\text{-}liq/Si\text{-}liq}$ that range from 1.59 to 2.01 for terrestrial systems (Veksler et al., 2006) and ~4 for lunar systems (Neal and Taylor, 1989). Therefore, using the reported abundances of high-K KREEP (which represents a mix of both the Fe-rich fraction and Si-rich fraction), we estimate an upper limit of 22 µg g^{-1} Sm and 10 µg g^{-1} Th for the urKREEP Si-rich fraction. Using this as a starting composition, batch partial melt trajectories for a Si-rich lithology that consists of plagioclase, K-feldspar, and Ca-phosphate were calculated; black and grey lines in Fig. 15a,b represent partial melt trajectories with 0.5 and 0.1 modal % Ca-phosphate, respectively, in the source lithology. A large range of D_{apt} values for both Th and Sm are reported in the literature; we plot partial melt trajectories using the maximum (1105) and minimum (84) values reported (see Supplementary Materials for details of the calculation and partition coefficients used). Regardless of the choice of D_{apt} value, it is clear that Ca-phosphate-bearing Si-rich source rocks can significantly fractionate Th/Sm relative to Ca-phosphate-free source rocks (red line; Fig. 15) during partial melting.

A challenge with arguing for a Si-rich source lithology is the potential difficulty in segregating immiscible melts within the urKREEP layer to ensure that only Si-rich rock types undergo partial melting. Despite the higher buoyancy of Si-rich melts relative to Fe-rich melts (Wilson and Head, 2003), the high viscosity of Si-rich melts means that they are unlikely to migrate large distances (Seddio et al., 2013; Valencia et al., 2024). Separation of Si-rich melts could be achieved if the Fe-rich fraction were sufficiently dense to sink into the mantle (similar to the proposed ilmenite-rich cumulate mantle overturn event; Elkins Tanton et al., 2002; Prissel et al., 2023). Despite this, partial melts from any Si-rich urKREEP lithologies would also have high viscosity and, as such, would also stay close to their source rocks at the crust/mantle interface. Only the largest lunar impact basins (e.g., the farside South Pole-Aitken or the postulated nearside Procellarum basin) would be able to exhume such material from the base of the crust (either ~30 km on the lunar nearside or ~60 km on the lunar farside; Wieczorek et al., 2013) to the near-surface, where it could be redistributed by later impact events.

Fertile mafic parental melt

Basaltic underplating requires the remelting of rock types such as KREEP basalts or alkali gabbronorites to produce silicic melts that have high incompatible trace element abundances (Gullikson et al., 2016; Valencia et al., 2024). Such KREEP-rich rocks are required to be coeval or older than the age of lunar granitoids (i.e., ~4.3 Ga). The dates reported here for three alkali gabbronorite samples (Table 1) have been affected by impact resetting and, as such, do not help constrain whether KREEP-rich rock types were present within the lunar crust at ~4.3 Ga. Consequently, we do not rule out basaltic underplating as a mechanism for generating felsic melts within the lunar crust.

For terrestrial systems, underplating has been estimated to produce 12 to 25 % partial melts from a mafic crust (Sisson et al., 2005). In a lunar context, which is generally considered to be more volatile-poor than terrestrial systems (e.g., Hui et al., 2013; Mills et al., 2016), the degree of melting could be lower. Using the $D_{Fe\text{-}liq/Si\text{-}liq}$ cited above, we estimated an upper limit of 37 µg g^{-1} Sm and 14 µg g^{-1} Th for the Fe-rich fraction (see Supplementary Materials Section S3). Using this starting composition, at partial melts < 25 %, modelling suggests that for a mafic mineral assemblage of plagioclase, pyroxene, and olivine, the resulting partial melts cannot fractionate Th/Sm to values higher than high-K KREEP (red line; Fig. 15c,d). Nevertheless, as seen in our felsic partial melt trajectories, the inclusion of phosphates in the source mineral assemblage (black and grey lines; Fig. 15c,d) has a significant effect, driving Th/Sm fractionation in the partial melt, regardless of the D_{apt} value used.

The deviation of trace element ratios away from high-K KREEP compositions (Warren, 1989) might reflect the crystallisation of Ca-phosphates within this system (e.g., Neal and Taylor, 1989). Not all granitoid fragments observed in our selected, or previously reported, samples contain Ca-phosphate; however, given the size of these samples, it is very likely that the modal mineral abundances are not representative of the rocks from which they were sourced (Warren, 2012). The abundance of Ca-phosphates is typically < 1 modal % for most rocks; therefore, we might not expect a ~200 µm granitoid fragment to contain Ca-phosphate grains. Crystallisation experiments reported by Gullikson et al. (2016) demonstrate that melts with a monzogabbro parental melt composition will crystallise a rock with ~2 modal % Ca-phosphate and an immiscible Si-rich melt that is within the range of reported bulk Apollo granitoid compositions. While such studies yield important insights into potential granitoid parent melts, there is a clear need to better understand how these magmatic systems partition trace elements during crystallisation, immiscible melt separation, and during partial melting of their source lithologies.

5 Conclusions

The impact-reworked nature of the granitoid and alkali gabbronorite fragments found within meteorites and the Apollo collection makes it challenging to decipher their crystallisation age(s). In many samples, the Rb-Sr, U-Pb and Pb-Pb chronometers do not record the crystallisation

age, but rather record resetting events. *In situ* Pb-Pb and Rb-Sr isotope measurements on plagioclase, K-feldspar, and Si-K-rich glass in granitoid clasts within Apollo samples 14303,330, 72275,520, and 73255,9083 are within error of the Imbrium impact event at 3.92 Ga. Granitoid clasts within samples 14305,111, 73235,73, 14305,102 record younger Rb-Sr and Pb-Pb dates, potentially reflecting modification by younger impacts at ~3.5 to ~3.6 Ga. Granitoid clasts within lunar meteorite sample NWA 4472 yield a date older than Imbrium (~4.14 Ga), potentially indicating only partial resetting by Imbrium at ~3.92 Ga, or full resetting by an older impact event.

The occurrence of Si-K-rich impact glass is common within Apollo granitoids. Dates calculated using Si-K-rich glass (using Si-K-rich glass only or glass and mineral isochrons) yield ages consistent with Imbrium, supporting their origin as impact glasses. We note that isochrons calculated using analyses from Si-K-rich glass from samples 14305,102 and 14304,209 yield significantly older dates (> 4.2 Ga). These samples also display isochron initial Sr isotope ratios below the expected growth from the lunar Sr isotope initial. This can be accounted for by variable Rb loss during impact melting, which would act to lower the $^{87}Rb/^{86}Sr$ of the resulting glass, resulting in steeper isochrons that regress to low initial Sr isotope ratios and yield spuriously old dates. These results highlight the potential limit of usefulness of the Rb-Sr systems for constraining the timing of impact glass generation.

Phosphate dates for alkali gabbronorite samples 14304,278 and 14313,70 yield dates (~ 3.93 Ga and 3.91 Ga, respectively) consistent with resetting by the Imbrium impact at ~3.92 Ga. For alkali gabbronorite sample 67975,9011, our Pb-Pb date (~3.56 Ga) indicates modification by an impact younger than Imbrium. For this sample, we report a phosphate-maskelynite Rb-Sr date that yields an older age (~3.94 Ga); however, it is unclear if Rb loss during shock transformation of feldspar to maskelynite has occurred, resulting in an apparent older age.

This work demonstrates that multi-geochronologic approaches are important for understanding the history of ancient, brecciated samples. We suggest that the U-Pb isotope systematics of zircon (while not commonly immune to impact shock resetting; Nemchin et al., 2008; Thiessen et al., 2018; Grange et al., 2013) remain our best tool for estimating the ages of lunar granitoid clasts. The majority of zircon-derived dates are older than crater counting age estimates of lunar silicic domes (Fig. 14; Shearer et al., 2023). As such, it remains unclear whether mechanisms capable of generating large volumes of felsic melts, such as crustal underplating by KREEP-rich mafic lithologies, are required to account for the formation of lunar silicic domes. This point is compounded by the lack of constraints on whether such KREEP-rich mafic lithologies, such as alkali gabbronorites, were present within the crust at ~4.3 Ga. Indeed, the original size of granitoid rocks from which the fragments available for study are sourced is uncertain; they could equally represent granophyre layers in differentiated magmatic intrusions or impact melt sheets. In either case, partial melt modelling indicates that melting of Ca-phosphates during partial melting of the source rocks, and/or the crystallisation of Ca-phosphates from the parental melt, is required to account for the unique incompatible trace element systematics recorded by granitoids relative to other lunar highland lithologies. Ultimately our understanding of the petrogenesis of lunar felsic rocks will be improved by future lunar missions targeting silicic dome sites (e.g., Lunar-VISE; Donaldson Hanna et al., 2023) and sites thought to be linked to surface exposures of granitoid-like rocks.

Acknowledgments

We thank the NASA AARB panel for the allocation of the sections used in this study, and the NASA JSC ARES curation staff for their help. We also thank Drs. Stewart Kearns and Jon Fellowes for help with the EPMA data collection, and Drs. John Cowpe and Lydia Fawcett for their help in the University of Manchester cleanroom labs. This project was funded with the support of Royal Society grants to J.F.S (URF\R1\211600; RF\ERE\210176) and to K.H.J (URF\R\201009 and RF\ERE\210158), in addition to STFC funding to K.H.J (ST/V000675/1, ST/Y002318/1) and to R.T.(ST/S002170/1), and NERC funding to D.A.N. (NE/T011106/1). We also thank the University of Manchester for funding the LA-ICP-MS facility. The NordSIMS facility is funded by Swedish Research Council infrastructure grant 2021-00276; this is NordSIMS publication #820. Finally, we thank Ryan Ickert and anonymous reviewers for their constructive reviews to help improve the manuscript.

Data, code, and outputs availability

Supplementary Text, Figures S1-S13 and Table S14 are available in the accompanying Supplementary Materials. All raw data reported here (Tables S1-S13), including the extended dataset for which only averages are reported in the text, can be found in the data publication of Pernet-Fisher (2026, https://doi.org/10.48420/29126819.v2). Main text figures and tables are available for download in the online version of this article.

Competing interests

The authors declare no competing interests.

Licence agreement

References

Albarède F (2009). Volatile accretion history of the terrestrial planets and dynamic implications. *Nature* 461(7268): 1227–1233. doi:10.1038/nature08477

Albee A, Burnett D, Chodos A, Haines E, Huneke J, Papanastassiou D, Wasserburg G (1970). Mineralogic and isotopic investigations on lunar rock 12013. *Earth and Planetary Science Letters* 9(2). doi:10.1016/0012-821x(70)90046-4

Anders E, Grevesse N (1989). Abundances of the elements: Meteoritic and solar. *Geochimica et Cosmochimica Acta* 53(1): 197–214. doi:10.1016/0016-7037(89)90286-x

Andrews-Hanna JC, Besserer J, Head III JW, Howett CJA, Kiefer WS, Lucey PJ, McGovern PJ, Melosh HJ, Neumann GA, Phillips RJ, Schenk PM, Smith DE, Solomon SC, Zuber MT (2014). Structure and evolution of the lunar Procellarum region as revealed by GRAIL gravity data. *Nature* 514(7520): 68–71. doi:10.1038/nature13697

Apen FE, Wall CJ, Cottle JM, Schmitz MD, Kylander-Clark AR, Seward GG (2022). Apatites for destruction: Reference apatites from Morocco and Brazil for U-Pb petrochronology and Nd and Sr isotope geochemistry. *Chemical Geology* 590: 120689. doi:10.1016/j.chemgeo.2021.120689

Arai T, Tomiyama T, Niihara T, Yokoyama T, Yoshitake M, Kaiden H, Misawa K, Irving AJ (2025). Multiple thermal events during 4350–3920 Ma recorded in a single lunar meteorite Northwest Africa 4485. *Icarus* 441: 116715. doi:10.1016/j.icarus.2025.116715

Barboni M, Needham E, Trail D, Bell EA, Chen HY (2025). Pervasive impact modification of pristine lunar clasts. *Nature Communications* 16(1). doi:10.1038/s41467-025-57691-z

Barboni M, Szymanowski D, Schoene B, Dauphas N, Zhang ZJ, Chen X, McKeegan KD (2024). High-precision U-Pb zircon dating identifies a major magmatic event on the Moon at 4.338 Ga. *Science Advances* 10(30). doi:10.1126/sciadv.adn9871

Barrett TJ, Robinson KL, Barnes JJ, Jeffrey Taylor G, Nagashima K, Huss GR, Franchi IA, Anand M, Kring DA (2023). Deciphering the origin(s) of H and Cl in Apollo 15 quartz monzodiorites: Evidence for multiple processes and reservoirs. *Geochimica et Cosmochimica Acta* 358: 192–206. doi:10.1016/j.gca.2023.08.004

Bevan D, Coath CD, Lewis J, Schwieters J, Lloyd N, Craig G, Wehrs H, Elliott T (2021). In situ Rb–Sr dating by collision cell, multicollection inductively-coupled plasma mass-spectrometry with pre-cell mass-filter, (CC-MC-ICPMS/MS). *Journal of Analytical Atomic Spectrometry* 36(5): 917–931. doi:10.1039/d1ja00006c

Binns RA (1967). Stony Meteorites bearing Maskelynite. *Nature* 213(5081): 1111–1112. doi:10.1038/2131111a0

Bischoff A, Stöffler D (1992). Shock metamorphism as a fundamental process in the evolution of planetary bodies: Information from meteorites. *European Journal of Mineralogy* 4(4): 707–756. doi:10.1127/ejm/4/4/0707

Borg LE, Carlson RW (2023). The Evolving Chronology of Moon Formation. *Annual Review of Earth and Planetary Sciences* 51(1): 25–52. doi:10.1146/annurev-earth-031621-060538

Borg LE, Edmunson JE, Asmerom Y (2005). Constraints on the U-Pb isotopic systematics of Mars inferred from a combined U-Pb, Rb-Sr, and Sm-Nd isotopic study of the Martian meteorite Zagami. *Geochimica et Cosmochimica Acta* 69(24): 5819–5830. doi:10.1016/j.gca.2005.08.007

Bray VJ, Tornabene LL, Keszthelyi LP, McEwen AS, Hawke BR, Giguere TA, Kattenhorn SA, Garry WB, Rizk B, Caudill CM, Gaddis LR, van der Bogert CH (2010). New insight into lunar impact melt mobility from the LRO camera. *Geophysical Research Letters* 37(21). doi:10.1029/2010gl044666

Cadogan PH (1974). Oldest and largest lunar basin? *Nature* 250(5464). doi:10.1038/250315a0

Černok A, White LF, Anand M, Tait KT, Darling JR, Whitehouse M, Miljković K, Lemelin M, Reddy SM, Fougerouse D, Rickard WDA, Saxey DW, Ghent R (2021). Lunar samples record an impact 4.2 billion years ago that may have formed the Serenitatis Basin. *Communications Earth & Environment* 2(1). doi:10.1038/s43247-021-00181-z

Černok A, White LF, Darling J, Dunlop J, Anand M (2019). Shock-induced microtextures in lunar apatite and merrillite. *Meteoritics & Planetary Science* 54(6): 1262–1282. doi:10.1111/maps.13278

Che X, Nemchin A, Liu D, Long T, Wang C, Norman MD, Joy KH, Tartese R, Head J, Jolliff B, Snape JF, Neal CR, Whitehouse MJ, Crow C, Benedix G, Jourdan F, Yang Z, Yang C, Liu J, Xie S, Bao Z, Fan R, Li D, Li Z, Webb SG (2021). Age and composition of young basalts on the Moon, measured from samples returned by Chang'e-5. *Science* 374(6569): 887–890. doi:10.1126/science.abl7957

Compston W, Foster J, Gray C (1977). Rb-Sr systematics in clasts and aphanites from consortium breccia 73215. *Lunar Science Conference Proceedings* 8: 2525–2549. bibcode:1977LPSC....8.2525C

Compston W, Williams IS, Meyer C (1984). U-Pb geochronology of zircons from lunar breccia 73217 using a sensitive high mass-resolution ion microprobe. *Journal of Geophysical Research: Solid Earth* 89(S02). doi:10.1029/jb089is02p0b525

Crow CA, McKeegan KD, Moser DE (2017). Coordinated U–Pb geochronology, trace element, Ti-in-zircon thermometry and microstructural analysis of Apollo zircons. *Geochimica et Cosmochimica Acta* 202: 264–284. doi:10.1016/j.gca.2016.12.019

Crow CA, Moser DE, McKeegan KD (2019). Shock metamorphic history of >4 Ga Apollo 14 and 15 zircons. *Meteoritics & Planetary Science* 54(1): 181–201. doi:10.1111/maps.13184

Delano J, Lindsley D, Rudowski R (1982). Glasses of impact origin from Apollo 11, 12, 15, and 16-Evidence for fractional vaporization and mare/highland mixing. *Lunar and Planetary Science Conference Proceedings* 12: 339–370. bibcode:1982LPSC...12..339D

Donaldson Hanna K, Benavente J, Bennett K, Denevi B, Dove A, Hagerty J, Team (2023). Lunar-VISE: An Investigation of the Moon's Non-Mare Silicic Volcanism. *Lunar and Planetary Science Conference Proceedings* 54: 2152. bibcode:2023LPICo2806.2152D

Downs R, Denton M (2006). Report on the Progress of the RRUFF Project: An Integrated Database of Raman Spectra, X-ray Diffraction, and Chemical Data for Minerals. *Gems & Gemology* 42(3): 89

Elkins Tanton LT, Van Orman JA, Hager BH, Grove TL (2002). Re-examination of the lunar magma ocean cumulate overturn hypothesis: melting or mixing is required. *Earth and Planetary Science Letters* 196(3-4): 239–249. doi:10.1016/s0012-821x(01)00613-6

Erickson T, Prissel K, Christoffersen R, Buckley W, Crow C, Eckley S, Valencia S (2024). Ternary Feldspar Within Felste Clasts From Apollo Impact Melt Breccia 72255. *Lunar and Planetary Science Conference Proceedings* 55: 1725. bibcode:2024LPICo3040.1725E

Evans AJ, Andrews-Hanna JC, Head JW, Soderblom JM, Solomon SC, Zuber MT (2018). Reexamination of Early Lunar Chronology With GRAIL Data: Terranes, Basins, and Impact Fluxes. *Journal of Geophysical Research: Planets* 123(7). doi:10.1029/2017je005421

Fagan TJ, Kashima D, Wakabayashi Y, Suginohara A (2014). Case study of magmatic differentiation trends on the Moon based on lunar meteorite Northwest Africa 773 and comparison with Apollo 15 quartz monzodiorite. *Geochimica et Cosmochimica Acta* 133: 97–127. doi:10.1016/j.gca.2014.02.025

Fassett CI, Head JW, Kadish SJ, Mazarico E, Neumann GA, Smith DE, Zuber MT (2012). Lunar impact basins: Stratigraphy, sequence and ages from superposed impact crater populations measured from Lunar Orbiter Laser Altimeter (LOLA) data. *Journal of Geophysical Research: Planets* 117(E12). doi:10.1029/2011je003951

First E, Rutherford M (2019). Silicate Liquid Immiscibility in Evolved Lunar Magmas. *Lunar and Planetary Science Conference Proceedings* 50: 2117. bibcode:2019LPI....50.2117F

Fritz J, Greshake A, Fernandes VA (2017). Revising the shock classification of meteorites. *Meteoritics & Planetary Science* 52(6): 1216–1232. doi:10.1111/maps.12845

Fuhrman M, Lindsley D (1988). Ternary-feldspar modeling and thermometry. *American mineralogist* 73(3-4): 201–215

Gaffney AM, Borg LE, Asmerom Y, Shearer CK, Burger PV (2011). Disturbance of isotope systematics during experimental shock and thermal metamorphism of a lunar basalt with implications for Martian meteorite chronology. *Meteoritics & Planetary Science* 46(1): 35–52. doi:10.1111/j.1945-5100.2010.01137.x

Ghiorso MS (1984). Activity/composition relations in the ternary feldspars. *Contributions to Mineralogy and Petrology* 87(3): 282–296. doi:10.1007/bf00373061

Gibson Jr EK, Hubbard NJ, Wiesmann H, Bansal BM, Moore GW (1973). How to lose Rb, K, and change the K/Rb ratio: An experimental study. In *Proceedings of the Lunar Science Conference*, vol. 4, p. 1263. Bibcode:1973LPSC....4.1263G

Giletti B (1991). Rb and Sr diffusion in alkali feldspars, with implications for cooling histories of rocks. *Geochimica et Cosmochimica Acta* 55(5): 1331–1343. doi:10.1016/0016-7037(91)90311-r

Grange M, Nemchin A, Pidgeon R, Timms N, Muhling J, Kennedy A (2009). Thermal history recorded by the Apollo 17 impact melt breccia 73217. *Geochimica et Cosmochimica Acta* 73(10): 3093–3107. doi:10.1016/j.gca.2009.02.032

Grange M, Pidgeon R, Nemchin A, Timms N, Meyer C (2013). Interpreting U–Pb data from primary and secondary features in lunar zircon. *Geochimica et Cosmochimica Acta* 101: 112–132. doi:10.1016/j.gca.2012.10.013

Greenwood JP, McSween HY (2001). Petrogenesis of Allan Hills 84001: Constraints from impact-melted feldspathic and silica glasses. *Meteoritics & Planetary Science* 36(1): 43–61. doi:10.1111/j.1945-5100.2001.tb01809.x

Gullikson AL, Hagerty JJ, Reid MR, Rapp JF, Draper DS (2016). Silicic lunar volcanism: Testing the crustal melting model. *American Mineralogist* 101(10): 2312–2321. doi:10.2138/am-2016-5619

Hagerty JJ, Lawrence DJ, Hawke BR, Vaniman DT, Elphic RC, Feldman WC (2006). Refined thorium abundances for lunar red spots: Implications for evolved, nonmare volcanism on the Moon. *Journal of Geophysical Research: Planets* 111(E6). doi:10.1029/2005je002592

Haskin L, Lindstrom M, Salpas P, Lindstrom D (1982). On compositional variations among lunar anorthosites. *Lunar and Planetary Science Conference Proceedings* 12: 41–66. bibcode:1982LPSC...12...41H

Hess P, Rutherford M, Guillemette R, Ryerson F, Tuchfeld H (1975). Residual products of fractional crystallization of lunar magmas-an experimental study. *Lunar Science Conference Proceedings* 6: 895–909. bibcode:1975LPSC....6..895H

Hirschmann M (1992). Origin of the Transgressive granophyres from the Layered Series of the Skaergaard intrusion, East Greenland. *Journal of Volcanology and Geothermal Research* 52(1-3). doi:10.1016/0377-0273(92)90140-9

Hogmalm KJ, Zack T, Karlsson AKO, Sjöqvist ASL, Garbe-Schönberg D (2017). In situ Rb–Sr and K–Ca dating by LA-ICP-MS/MS: an evaluation of N2O and SF6 as reaction gases. *Journal of Analytical Atomic Spectrometry* 32(2): 305–313. doi:10.1039/c6ja00362a

Holtz F, Johannes W (1991). Genesis of Peraluminous Granites I. Experimental Investigation of Melt Compositions at 3 and 5 kb and Various H2O Activities. *Journal of Petrology* 32(5): 935–958. doi:10.1093/petrology/32.5.935

Hou K, Qin Y, Li Y, Fan C (2013). In situ Sr-Nd isotopic measurement of apatite using laser ablation multi-collector inductively coupled plasma-mass spectrometry. *Rock and Mineral Analysis* 32: 547–554

Hui H, Peslier AH, Zhang Y, Neal CR (2013). Water in lunar anorthosites and evidence for a wet early Moon. *Nature Geoscience* 6(3): 177–180. doi:10.1038/ngeo1735

Hurwitz DM, Kring DA (2014). Differentiation of the South Pole–Aitken basin impact melt sheet: Implications for lunar exploration. *Journal of Geophysical Research: Planets* 119(6). doi:10.1002/2013je004530

Ivanov M, Head J, Bystrov A (2016). The lunar Gruithuisen silicic extrusive domes: Topographic configuration, morphology, ages, and internal structure. *Icarus* 273. doi:10.1016/j.icarus.2015.12.015

Jaret SJ, Woerner WR, Phillips BL, Ehm L, Nekvasil H, Wright SP, Glotch TD (2015). Maskelynite formation via solid-state transformation: Evidence of infrared and X-ray anisotropy. *Journal of Geophysical Research: Planets* 120(3): 570–587. doi:10.1002/2014je004764

Jegal Y, Zimmermann C, Reisberg L, Yeghicheyan D, Cloquet C, Peiffert C, Gerardin M, Deloule E, Mercadier J (2022). Characterisation of Reference Materials for In Situ Rb-Sr Dating by LA-ICP-MS/MS. *Geostandards and Geoanalytical Research* 46(4): 645–671. doi:10.1111/ggr.12456

Jessberger E, Staudacher T, Dominik B, Kirsten T (1978). Argon-argon ages of aphanite samples from consortium breccia 73255. *Lunar and Planetary Science Conference Proceedings* 9: 841–854. bibcode:1978LPSC....9..841J

Jochum KP, Nohl U (2008). Reference materials in geochemistry and environmental research and the GeoReM database. *Chemical Geology* 253(1-2). doi:10.1016/j.chemgeo.2008.04.002

Jochum KP, Wilson SA, Abouchami W, Amini M, Chmeleff J, Eisenhauer A, Hegner E, Iaccheri LM, Kieffer B, Krause J, McDonough WF, Mertz-Kraus R, Raczek I, Rudnick RL, Scholz D, Steinhoefel G, Stoll B, Stracke A, Tonarini S, Weis D, Weis U, Woodhead JD (2011). GSD-1G and MPI-DING Reference Glasses for In Situ and Bulk Isotopic Determination. *Geostandards and Geoanalytical Research* 35(2): 193–226. doi:10.1111/j.1751-908x.2010.00114.x

Jolliff BL, Korotev RL, Haskin LA (1991). A ferroan region of the lunar highlands as recorded in meteorites MAC88104 and MAC88105. *Geochimica et Cosmochimica Acta* 55(11): 3051–3071. doi:10.1016/0016-7037(91)90473-i

Joy K, Burgess R, Hinton R, Fernandes V, Crawford I, Kearsley A, Irving A (2011). Petrogenesis and chronology of lunar meteorite Northwest Africa 4472: A KREEPy regolith breccia from the Moon. *Geochimica et Cosmochimica Acta* 75(9): 2420–2452. doi:10.1016/j.gca.2011.02.018

Joy KH, Wang N, Snape JF, Goodwin A, Pernet-Fisher JF, Whitehouse MJ, Liu Y, Lin YT, Darling JR, Tar P, Tartèse R (2024). Evidence of a 4.33 billion year age for the Moon's South Pole–Aitken basin. *Nature Astronomy* 9(1): 55–65. doi:10.1038/s41550-024-02380-y

Keays RR, Lightfoot PC (2020). Mafic intrusions in the footwall of the Sudbury Igneous Complex: Origin of the Sudbury impact melt sheet and its associated ore deposits. *Ore Geology Reviews* 120: 103435. doi:10.1016/j.oregeorev.2020.103435

Kennedy AK, Wotzlaw J, Crowley JL, Schmitz M, Schaltegger U, Wade B, Martin L, Talavera C, Ware B, Bui TH (2023). Apatite Reference Materials for SIMS Microanalysis of Isotopes and Trace Elements. *Geostandards and Geoanalytical Research* 47(2): 373–402. doi:10.1111/ggr.12477

Kirsten T, Deubner J, Ducati H, Gentner W, Horn P, Jessberger E, Kalbitzer S, Kaneoka I, Kiko J, Krätschmer W, Müller HW, Plieninger S T andThio (1972). Rare gases and ion tracks in individual components and bulk samples of Apollo 14 and 15 fines and fragmental rocks. *Lunar and Planetary Science Conference Proceedings* 3: 452–454. bibcode:1972LPI.....3..452K

Korotev RL, Jolliff BL, Zeigler RA, Gillis JJ, Haskin LA (2003). Feldspathic lunar meteorites and their implications for compositional remote sensing of the lunar surface and the composition of the lunar crust. *Geochimica et Cosmochimica Acta* 67(24): 4895–4923. doi:10.1016/j.gca.2003.08.001

Korotev RL, Zeigler RA, Floss C (2010). On the origin of impact glass in the Apollo 16 regolith. *Geochimica et Cosmochimica Acta* 74(24): 7362–7388. doi:10.1016/j.gca.2010.09.020

Kring D, McGovern P, Potter R, Collins G, Grange M, Nemchin A (2015). Was an Epoch of Lunar Magmatism Triggered by the South Pole-Aitken Basin Impact? *Lunar and Planetary Science Conference Proceedings* 55: 3009. bibcode:2015LPICo1826.3009K

Lamadrid H, Lamb W, Santosh M, Bodnar R (2014). Raman spectroscopic characterization of H2O in CO2-rich fluid inclusions in granulite facies metamorphic rocks. *Gondwana Research* 26(1). doi:10.1016/j.gr.2013.07.003

Li C, Hu H, Yang MF, Liu J, Zhou Q, Ren X, Liu B, Liu D, Zeng X, Zuo W, Zhang G, Zhang H, Yang S, Wang Q, Deng X, Gao X, Su Y, Wen W, Ouyang Z (2024). Nature of the lunar far-side samples returned by the Chang'E-6 mission. *National Science Review* 11(11). doi:10.1093/nsr/nwae328

Li QL, Zhou Q, Liu Y, Xiao Z, Lin Y, Li JH, Ma HX, Tang GQ, Guo S, Tang X, Yuan JY, Li J, Wu FY, Ouyang Z, Li C, Li XH (2021). Two-billion-year-old volcanism on the Moon from Chang'e-5 basalts. *Nature* 600(7887): 54–58. doi:10.1038/s41586-021-04100-2

Li Y, Wang Z, Zhang W, Zhou L, Zong K, Feng L, Li J, He Q, She Z, Wu X, Hu Z, Xiao L, Wu Y, Liu Y (2023). Rb-Sr isotopes record complex thermal modification of Chang'e-5 lunar soils. *Science Bulletin* 68(22): 2724–2728. doi:10.1016/j.scib.2023.09.045

Liaw Cw, Liu TC, Iizuka Y, Yang HY (2006). Anhydrous Melting and Crystallization of Granite from the Transition Zone of the Qilian Orogenic Belt, NW China: An Experimental Study at Atmospheric Pressure. *Terrestrial, Atmospheric and Oceanic Sciences* 17(1): 233. doi:10.3319/tao.2006.17.1.233(tt)

Lindstrom MM, Lindstrom DJ (1986). Lunar granulites and their precursor anorthositic norites of the early lunar crust. *Journal of Geophysical Research: Solid Earth* 91(B4): 263–276. doi:10.1029/jb091ib04p0d263

Lodders K (2003). Solar System Abundances and Condensation Temperatures of the Elements. *The Astrophysical Journal* 591(2): 1220–1247. doi:10.1086/375492

Meyer C (2011). Lunar Sample Compendium. bibcode:2005STIN...0611039M

Meyer C, Williams I, Compston W (1989). Pb207/Pb206 Ages of Zircon-containing Rock Fragments Indicate Continuous Magmatism in the Lunar Crust from 4350 to 3900 Million Years. *Abstracts of the Lunar and Planetary Science Conference* 20: 691–692. bibcode:1989LPI....20..691M

Meyer C, Williams IS, Compston W (1996). Uranium-lead ages for lunar zircons: Evidence for a prolonged period of granophyre formation from 4.32 to 3.88 Ga. *Meteoritics & Planetary Science* 31(3): 370–387. doi:10.1111/j.1945-5100.1996.tb02075.x

Mills R, Simon J, Alexander C, Wang J, Hauri E (2016). Water in alkali feldspar: The effect of rhyolite generation on the lunar hydrogen budget. *Geochemical Perspectives Letters* p. 115–123. doi:10.7185/geochemlet.1712

Mittlefehldt DW (1994). ALH84001, a cumulate orthopyroxenite member of the martian meteorite clan. *Meteoritics* 29(2): 214–221. doi:10.1111/j.1945-5100.1994.tb00673.x

Morgan GB, London D (2003). Trace-element partitioning at conditions far from equilibrium: Ba and Cs distributions between alkali feldspar and undercooled hydrous granitic liquid at 200 MPa. *Contributions to Mineralogy and Petrology* 144(6): 722–738. doi:10.1007/s00410-002-0425-y

Neal C, Taylor L (1989). The nature of barium partitioning between immiscible melts: a comparison of experimental and natural systems with reference to lunar granite petrogenesis. *Lunar and Planetary Science Conference Proceedings* 19: 209–218. bibcode:1989LPSC...19..209N

Nebel O, Mezger K (2006). Reassessment of the NBS SRM-607 K-feldspar as a high precision Rb/Sr and Sr isotope reference. *Chemical Geology* 233(3-4): 337–345. doi:10.1016/j.chemgeo.2006.03.003

Nemchin A, Jeon H, Bellucci J, Timms N, Snape J, Kilburn M, Whitehouse M (2017). Pb-Pb ages of feldspathic clasts in two Apollo 14 breccia samples. *Geochimica et Cosmochimica Acta* 217: 441–461. doi:10.1016/j.gca.2017.08.024

Nemchin A, Pidgeon R, Whitehouse M, Vaughan J, Meyer C (2008). SIMS U–Pb study of zircon from Apollo 14 and 17 breccias: Implications for the evolution of lunar KREEP. *Geochimica et Cosmochimica Acta* 72(2): 668–689. doi:10.1016/j.gca.2007.11.009

Nemchin AA, Long T, Jolliff BL, Wan Y, Snape JF, Zeigler R, Grange ML, Liu D, Whitehouse MJ, Timms NE, Jourdan F (2021). Ages of lunar impact breccias: Limits for timing of the Imbrium impact. *Geochemistry* 81(1): 125683. doi:10.1016/j.chemer.2020.125683

Newton RC (1986). *Fluids of Granulite Facies Metamorphism*, p. 36–59. Springer New York. doi:10.1007/978-1-4612-4896-5_2

Nimmo F, Kleine T, Morbidelli A (2024). Tidally driven remelting around 4.35 billion years ago indicates the Moon is old. *Nature* 636(8043): 598–602. doi:10.1038/s41586-024-08231-0

Norman MD, Bennett VC, Ryder G (2002). Targeting the impactors: siderophile element signatures of lunar impact melts from Serenitatis. *Earth and Planetary Science Letters* 202(2). doi:10.1016/s0012-821x(02)00780-x

Ofierska W, Schmidt MW, Liebske C, Sossi PA (2026). Final differentiation of the lunar magma ocean: genesis of KREEP and the limited role of silicate liquid immiscibility. *Earth and Planetary Science Letters* 673: 119691. doi:10.1016/j.epsl.2025.119691

Oliveira BH, Snape JF, Tartèse R, Pernet-Fisher JF, van Acken D, Whitehouse MJ, Joy KH (2025). Insights on the volcanic and impact histories of the lunar nearside from the petrology, geochemistry, and geochronology of the Calcalong Creek lunar regolith breccia meteorite. *Meteoritics & Planetary Science* 60(3): 392–421. doi:10.1111/maps.14305

Papike J, Fowler G, Shearer C (1997). Evolution of the lunar crust: SIMS study of plagioclase from ferroan anorthosites. *Geochimica et Cosmochimica Acta* 61(11): 2343–2350. doi:https://doi.org/10.1016/S0016-7037(97)00086-0

Papike JJ, Ryder G, Shearer CK (1998). *Lunar Samples*, p. 719–952. De Gruyter. doi:10.1515/9781501508806-020

Paton C, Hellstrom J, Paul B, Woodhead J, Hergt J (2011). Iolite: Freeware for the visualisation and processing of mass spectrometric data. *Journal of Analytical Atomic Spectrometry* 26(12): 2508. doi:10.1039/c1ja10172b

Pernet-Fisher J (2026). In situ Rb-Sr, U-Pb, and Pb isotope systematics for granitoid and alkali gabbronorite samples from Apollo landing sites and regolith breccia meteorite Northwest Africa (NWA) 4472. Version 2. University of Manchester. doi:10.48420/29126819.v2

Pernet-Fisher J, Howarth G, Liu Y, Chen Y, Taylor L (2014). Estimating the lunar mantle water budget from phosphates: Complications associated with silicate-liquid-immiscibility. *Geochimica et Cosmochimica Acta* 144: 326–341. doi:10.1016/j.gca.2014.09.004

Pernet-Fisher JF, Joy KH, Nottingham M, Hartley ME, Tartèse R (2024). Constraining the Protoliths of the Apollo Granulite Suite. *The Planetary Science Journal* 5(12): 278. doi:10.3847/psj/ad86c5

Petrishcheva E, Tiede L, Schweinar K, Habler G, Li C, Gault B, Abart R (2020). Spinodal decomposition in alkali feldspar studied by atom probe tomography. *Physics and Chemistry of Minerals* 47(7). doi:10.1007/s00269-020-01097-4

Phinney D, Kahl S, Reynolds J (1975). 40Ar-39Ar dating of Apollo 16 and 17 rocks. *In: Lunar Science Conference, 6th* 6: 1593–1608. bibcode:1975LPSC....6.1593P

Pidgeon R, Aftalion M (1978). Cogenetic and inherited zircon U–Pb systems in granites: Palaeozoic granites of Scotland and England. In Bowes DR, Leake B (eds.) *Crustal evolution in northwestern Britain and adjacent areas, Geological Journal Special Issue*, 10, p. 183–220. Liverpool: Seel House Press

Potts NJ, Tartèse R, Anand M, van Westrenen W, Griffiths AA, Barrett TJ, Franchi IA (2016). Characterization of mesostasis regions in lunar basalts: Understanding late-stage melt evolution and its influence on apatite formation. *Meteoritics & Planetary Science* 51(9). doi:10.1111/maps.12681

Prissel TC, Zhang N, Jackson CRM, Li H (2023). Rapid transition from primary to secondary crust building on the Moon explained by mantle overturn. *Nature Communications* 14(1). doi:10.1038/s41467-023-40751-7

Quick J, Albee A, Ma M, Murali A, Schmitt R (1977). Chemical compositions and possible immiscibility of two silicate melts in 12013. *Lunar Science Conference Proceedings* 8: 2153–2189. bibcode:1977LPSC....8.2153Q

Quick J, James O, Albee A (1982). Petrology and petrogenesis of lunar breccia 12013. *Lunar and Planetary Science Conference Proceedings* 12: 117–172. bibcode:1982LPSC...12..117Q

Ravi S, Till CB, Robinson MS (2025). On the Origin of Silicic Magmas on the Moon. *The Planetary Science Journal* 6(9): 223. doi:10.3847/psj/adf7a4

Redaa A, Farkaš J, Gilbert S, Collins AS, Löhr S, Vasegh D, Forster M, Blades M, Zack T, Giuliani A, Maas R, Baldermann A, Dietzel M, Garbe-Schönberg D (2023). Testing Nano-Powder and Fused-Glass Mineral Reference Materials for In Situ Rb-Sr Dating of Glauconite, Phlogopite, Biotite and Feldspar via LA-ICP-MS/MS. *Geostandards and Geoanalytical Research* 47(1): 23–48. doi:10.1111/ggr.12467

Robertson JK, Wyllie PJ (1971). Experimental Studies on Rocks from the Deboullie Stock, Northern Maine, including Melting Relations in the Water-Deficient Environment. *The Journal of Geology* 79(5). doi:10.1086/627675

Roedder E, Weiblen P (1971). Petrology of silicate melt inclusions, Apollo 11 and Apollo 12 and terrestrial equivalents. *Lunar Science Conference Proceedings* 2: 507–528. bibcode:1971LPSC....2..507R

Roedder E, Weiblen PW (1970). Silicate Liquid Immiscibility in Lunar Magmas, Evidenced by Melt Inclusions in Lunar Rocks. *Science* 167(3918): 641–644. doi:10.1126/science.167.3918.641

Rundle C (1982). The Chronology of Igneous Intrusion in the English Lake District, Unpublished PhD thesis, University of London, UK

Rutherford M, Hess P, Ryerson F, Campbell H, Dick P (1976). The chemistry, origin and petrogenetic implications of lunar granite and monzonite. *Lunar Science Conference Proceedings* 7: 1723–1740. bibcode:1976LPSC....7.1723R

Ruzicka A (1995). Nullarbor 018: A new L6 chondrite from Australia. *Meteoritics* 30(1): 102–105. doi:10.1111/j.1945-5100.1995.tb01216.x

Ryder G, Spudis P (1987). Chemical composition and origin of Apollo 15 impact melts. *Journal of Geophysical Research: Solid Earth* 92(B4). doi:10.1029/jb092ib04p0e432

Ryder G, Stoeser D, Marvin U, Bower J (1975). Lunar granites with unique ternary feldspars. *Lunar Science Conference Proceedings* 6: 435–449. bibcode:1975LPSC....6..435R

Rösel D, Zack T (2022). LA-ICP-MS/MS Single-Spot Rb-Sr Dating. *Geostandards and Geoanalytical Research* 46(2): 143–168. doi:10.1111/ggr.12414

Schärer U, Deutsch A (1990). Isotope systematics and shock-wave metamorphism: II. U-Pb and Rb-Sr in naturally shocked rocks; the Haughton Impact Structure, Canada. *Geochimica et Cosmochimica Acta* 54(12): 3435–3447. doi:10.1016/0016-7037(90)90296-w

Scott ERD, Yamaguchi A, Krot AN (1997). Petrological evidence for shock melting of carbonates in the martian meteorite ALH84001. *Nature* 387(6631): 377–379. doi:10.1038/387377a0

Seddio SM, Jolliff BL, Korotev RL, Zeigler RA (2013). Petrology and geochemistry of lunar granite 12032,366-19 and implications for lunar granite petrogenesis. *American Mineralogist* 98(10): 1697–1713. doi:10.2138/am.2013.4330

Seddio SM, Korotev RL, Jolliff BL, Wang A (2015). Silica polymorphs in lunar granite: Implications for granite petrogenesis on the Moon. *American Mineralogist* 100(7). doi:10.2138/am-2015-5058

Shearer C, Neal CR, Glotch TD, Prissel TC, Bell AS, Fernandes VA, Gaddis LR, Jolliff BL, Laneuville M, Magna T, Simon J (2023). Magmatic Evolution II: A New View of Post-Differentiation Magmatism. *Reviews in Mineralogy and Geochemistry* 89(1): 147–206. doi:10.2138/rmg.2023.89.04

Shearer CK, Simon SB, Jolliff BL, McCubbin FM, Cato M, Borg L, Marks N, Jacobsen B, Simon JI, Christofferson R, Erickson T, Hahn T, Petro N, Tartese R, Anand M, Team AS (2022). A "New" Lunar Sample Return Mission Investigates Silicic Magmatism Recorded by Lithic Fragments from Double Drive Tube 73001/73002. *Apollo 17-ANGSA Workshop* 2704: 2004. bibcode:2022LPICo2704.2004S

Shervais J, Taylor L (1983). Micrographic granite: more from Apollo 14. *Lunar and Planetary Science Conference Proceedings* 14: 696–697. bibcode:1983LPI....14..696S

Shervais JW, McGee JJ (1999). Petrology of the Western Highland Province: Ancient crust formation at the Apollo 14 site. *Journal of Geophysical Research: Planets* 104(E3): 5891–5920. doi:10.1029/1998je900025

Shih CY, Nyquist L, Bogard D, Wiesmann H (1994). K-Ca and Rb-Sr dating of two lunar granites: Relative chronometer resetting. *Geochimica et Cosmochimica Acta* 58(14). doi:10.1016/0016-7037(94)90182-1

Shih CY, Nyquist L, Bogard D, Wooden J, Bansal B, Wiesmann H (1985). Chronology and petrogenesis of a 1.8 g lunar granitic clast: 14321, 1062. *Geochimica et Cosmochimica Acta* 49(2): 411–426. doi:10.1016/0016-7037(85)90033-x

Simon J, Christoffersen R, Wang J, Mouser M, Mills R, Ross D, Rahman Z, Alexander C (2020). Volatiles in lunar felsite clasts: Impact-related delivery of hydrous material to an ancient dry lunar crust. *Geochimica et Cosmochimica Acta* 276: 299–326. doi:10.1016/j.gca.2020.02.008

Simon J, Shih C, Nyquist L (2011). K-Ca and Rb-Sr dating of lunar granite 14321 revisited. *Lunar and Planetary Science Conference Proceedings* 42. bibcode:2011LPI....42.2754S

Sisson TW, Ratajeski K, Hankins WB, Glazner AF (2005). Voluminous granitic magmas from common basaltic sources. *Contributions to Mineralogy and Petrology* 148(6): 635–661. doi:10.1007/s00410-004-0632-9

Smith J, Steele I (1984). Chemical substitution in silica polymorphs. *Neues Jahrbuch für Mineralogie Monatshefte* 3: 137–144

Snape JF, Nemchin AA, Bellucci JJ, Whitehouse MJ, Tartèse R, Barnes JJ, Anand M, Crawford IA, Joy KH (2016). Lunar basalt chronology, mantle differentiation and implications for determining the age of the Moon. *Earth and Planetary Science Letters* 451: 149–158. doi:10.1016/j.epsl.2016.07.026

Snape JF, Nemchin AA, Whitehouse MJ, Li QL, Liu Y, Timms NE, Erickson T, Benedix GK (2024). Post-Imbrium Pb–Pb isochron ages for Apollo basaltic impact melt samples 14078 and 68415. *Royal Society Open Science* 11(5). doi:10.1098/rsos.231963

Snape JF, Nemchin AA, Whitehouse MJ, Merle RE, Hopkinson T, Anand M (2019). The timing of basaltic volcanism at the Apollo landing sites. *Geochimica et Cosmochimica Acta* 266: 29–53. doi:10.1016/j.gca.2019.07.042

Snyder GA, Taylor LA, Halliday AN (1995). Chronology and petrogenesis of the lunar highlands alkali suite: Cumulates from KREEP basalt crystallization. *Geochimica et Cosmochimica Acta* 59(6): 1185–1203. doi:10.1016/0016-7037(95)00034-w

Sossi PA, Klemme S, O'Neill HS, Berndt J, Moynier F (2019). Evaporation of moderately volatile elements from silicate melts: experiments and theory. *Geochimica et Cosmochimica Acta* 260. doi:10.1016/j.gca.2019.06.021

Stacey J, Kramers J (1975). Approximation of terrestrial lead isotope evolution by a two-stage model. *Earth and Planetary Science Letters* 26(2). doi:10.1016/0012-821x(75)90088-6

Stöffler D, Langenhorst F (1994). Shock metamorphism of quartz in nature and experiment: I. Basic observation and theory*. *Meteoritics* 29(2): 155–181. doi:10.1111/j.1945-5100.1994.tb00670.x

Stöffler D, Ostertag R, Jammes C, Pfannschmidt G, Gupta P, Simon S, Papike J, Beauchamp R (1986). Shock metamorphism and petrography of the Shergotty achondrite. *Geochimica et Cosmochimica Acta* 50(6): 889–903. doi:10.1016/0016-7037(86)90371-6

Stöffler D, Ryder G, Ivanov B, Artemieva N, Cintala M, Grieve R (2006). Cratering History and Lunar Chronology. *Reviews in Mineralogy and Geochemistry* 60(1): 519–596. doi:10.2138/rmg.2006.60.05

Su B, Chen Y, Wang Z, Zhang D, Chen H, Gou S, Yue Z, Liu Y, Yuan J, Tang G, Guo S, Li Q, Lin YT, Li XH, Wu FY (2025). South Pole–Aitken massive impact 4.25 billion years ago revealed by Chang'e-6 samples. *National Science Review* 12(6). doi:10.1093/nsr/nwaf103

Su B, Chen Y, Yue Z, Chen L, Mitchell RN, Tang M, Yang W, Huang G, Guo J, Li XH, Wu FY (2023). Crustal remelting origin of highly silicic magmatism on the Moon. *Communications Earth & Environment* 4(1). doi:10.1038/s43247-023-00900-8

Taylor S (1982). *Planetary science: A lunar perspective*. Lunar and Planetary Institute, Houston. bibcode:1982ntrs.book31518T

Thiessen F, Nemchin A, Snape J, Bellucci J, Whitehouse M (2018). Apollo 12 breccia 12013: Impact-induced partial Pb loss in zircon and its implications for lunar geochronology. *Geochimica et Cosmochimica Acta* 230. doi:10.1016/j.gca.2018.03.023

Thomas JB, Bruce Watson E, Spear FS, Shemella PT, Nayak SK, Lanzirotti A (2010). TitaniQ under pressure: the effect of pressure and temperature on the solubility of Ti in quartz. *Contributions to Mineralogy and Petrology* 160(5): 743–759. doi:10.1007/s00410-010-0505-3

Timms NE, Kinny PD, Reddy SM, Evans K, Clark C, Healy D (2011). Relationship among titanium, rare earth elements, U–Pb ages and deformation microstructures in zircon: Implications for Ti-in-zircon thermometry. *Chemical Geology* 280(1-2): 33–46. doi:10.1016/j.chemgeo.2010.10.005

Trail D, Barboni M, McKeegan KD (2020). Evidence for diverse lunar melt compositions and mixing of the pre-3.9 Ga crust from zircon chemistry. *Geochimica et Cosmochimica Acta* 284. doi:10.1016/j.gca.2020.06.018

Turner G, Cadogan P (1975). The history of lunar basin formation inferred from 40Ar-39Ar dating of highland rocks. *Lunar and Planetary Science Conference Proceedings* 6: 826–828. bibcode:1975LPI.....6..826T

Tuttle OF, Bowen NL (1958). *Origin of granite in the light of experimental studies in the system NaAlSi3O8–KAlSi3O8–SiO2–H2O*. Geological Society of America. doi:10.1130/mem74-p1

Valencia S, Korotev R, Jolliff B (2024). Compositional analysis of Apollo 12 Granitic Breccia 12013: Insights into protoliths and formation. *Geochimica et Cosmochimica Acta* 367: 189–212. doi:10.1016/j.gca.2023.12.034

Valley JW, Spicuzza MJ, Ushikubo T (2013). Correlated δ18O and [Ti] in lunar zircons: a terrestrial perspective for magma temperatures and water content on the Moon. *Contributions to Mineralogy and Petrology* 167(1). doi:10.1007/s00410-013-0956-4

Veksler IV, Dorfman AM, Danyushevsky LV, Jakobsen JK, Dingwell DB (2006). Immiscible silicate liquid partition coefficients: implications for crystal-melt element partitioning and basalt petrogenesis. *Contributions to Mineralogy and Petrology* 152(6): 685–702. doi:10.1007/s00410-006-0127-y

Vermeesch P (2018). IsoplotR: A free and open toolbox for geochronology. *Geoscience Frontiers* 9(5). doi:10.1016/j.gsf.2018.04.001

Villa IM, Holden NE, Possolo A, Ickert RB, Hibbert DB, Renne PR, Bonardi ML, De Bièvre P (2022). IUGS–IUPAC recommendations and status reports on the half-lives of 87Rb. *Pure and Applied Chemistry* 94(9). doi:10.1515/pac-2021-1202

Wadge AJ, Gale NH, Beckinsale CC R D Rundle (1978). A Rb-Sr isochron for the Shap Granite. *Proceedings of the Yorkshire Geological Society* 42(2). doi:10.1144/pygs.42.2.297

Wagner R, Head JW, Wolf U, Neukum G (2002). Stratigraphic sequence and ages of volcanic units in the Gruithuisen region of the Moon. *Journal of Geophysical Research: Planets* 107(E11). doi:10.1029/2002je001844

Wark DA, Watson EB (2006). TitaniQ: a titanium-in-quartz geothermometer. *Contributions to Mineralogy and Petrology* 152(6). doi:10.1007/s00410-006-0132-1

Warner R, Taylor G, Mansker W, Keil K (1978). Clast assemblages of possible deep-seated (77517) and immiscible-melt (77538) origins in Apollo 17 breccias. *Lunar and Planetary Science Conference Proceedings* 9: 941–958. bibcode:1978LPSC....9..941W

Warren P (1989). KREEP: major-element diversity, trace element uniformity (almost). *Workshop on Moon in Transition: Apollo 14, KREEP, and Evolved Lunar Rocks* p. 149–153. bibcode:1989mtak.conf..149W

Warren P (2012). Let's get real: not every lunar rock sample is big enough to be representative for every purpose. *Second conference on the Lunar Highlands crust* p. 59–60. bibcode:2012LPICo1677...59W

Warren PH, Jerde EA, Kallemeyn GW (1987). Pristine Moon rocks: A "large" felsite and a metal-rich ferroan anorthosite. *Journal of Geophysical Research: Solid Earth* 92(B4). doi:10.1029/jb092ib04p0e303

Warren PH, Taylor GJ, Keil K, Shirley DN, Wasson JT (1983). Petrology and chemistry of two "large" granite clasts from the moon. *Earth and Planetary Science Letters* 64(2): 175–185. doi:10.1016/0012-821x(83)90202-9

Watson EB (1976). Two-liquid partition coefficients: Experimental data and geochemical implications. *Contributions to Mineralogy and Petrology* 56(1): 119–134. doi:10.1007/bf00375424

Wenk HR, Bulakh A (2016). *Minerals: Their Constitution and Origin*. Cambridge University Press. doi:10.1017/9781316226889

Whitaker E (1981). The lunar Procellarum basin. In *Multi-ring basins: Formation and evolution, Proceedings of the Lunar and Planetary Science Conference*, vol. 12A, p. 105–111. bibcode:1981mrbf.conf..105W

Wieczorek MA, Neumann GA, Nimmo F, Kiefer WS, Taylor GJ, Melosh HJ, Phillips RJ, Solomon SC, Andrews-Hanna JC, Asmar SW, Konopliv AS, Lemoine FG, Smith DE, Watkins MM, Williams JG, Zuber MT (2013). The Crust of the Moon as Seen by GRAIL. *Science* 339(6120): 671–675. doi:10.1126/science.1231530

Wilhelms DE, McCauley JF, Trask NJ (1987). *The geologic history of the Moon*. U.S. Geological Survey. doi:10.3133/pp1348

Wilson L, Head JW (2003). Lunar Gruithuisen and Mairan domes: Rheology and mode of emplacement. *Journal of Geophysical Research: Planets* 108(E2). doi:10.1029/2002je001909

Woodhead JD, Hergt JM (2000). Pb-Isotope Analyses of USGS Reference Materials. *Geostandards Newsletter* 24(1): 33–38. doi:10.1111/j.1751-908x.2000.tb00584.x

Woodhead JD, Hergt JM (2001). Strontium, Neodymium and Lead Isotope Analyses of NIST Glass Certified Reference Materials: SRM 610, 612, 614. *Geostandards Newsletter* 25(2-3): 261–266. doi:10.1111/j.1751-908x.2001.tb00601.x

Yamaguchi A, Karouji Y, Takeda H, Nyquist L, Bogard D, Ebihara M, Shih CY, Reese Y, Garrison D, Park J, McKay G (2010). The variety of lithologies in the Yamato-86032 lunar meteorite: Implications for formation processes of the lunar crust. *Geochimica et Cosmochimica Acta* 74(15): 4507–4530. doi:10.1016/j.gca.2010.04.015

Yang Y, Jiang T, Liu Y, Xu Y, Zhang H, Tian H, Yang W, Zou Y (2022). A Micro Mid-Infrared Spectroscopic Study of Chang'e-5 Sample. *Journal of Geophysical Research: Planets* 127(8). doi:10.1029/2022je007453

Zeng X, Joy KH, Li S, Lin Y, Wang N, Li X, Li Y, Hao J, Liu J, Wang S (2020). Oldest Immiscible Silica-rich Melt on the Moon Recorded in a 4.38 Ga Zircon. *Geophysical Research Letters* 47(4). doi:10.1029/2019gl085997

Zeng X, Li X, Xia X, Liu J, Cui Z, Yu W, Ouyang Z (2021). New Evidence for 4.32 Ga Ancient Silicic Volcanism on the Moon. *Geophysical Research Letters* 48(13). doi:10.1029/2021gl092639

Zhang L, Yang YN, Wang J, Cui ZX, Wang CY, He PL, Zhang YQ, Lin M, Xu YG (2025). Silicate liquid immiscibility in the Chang'e 5 lunar mare magmas: Constraints on the petrogenesis of lunar granitic rocks. *American Mineralogist* 110(9): 1462–1471. doi:10.2138/am-2024-9577

Zhang Y, Charlier B, Krein SB, Grove TL, Namur O, Holtz F (2024). The very late-stage crystallization of the lunar magma ocean and the composition of immiscible urKREEP. *Earth and Planetary Science Letters* 646: 118989. doi:10.1016/j.epsl.2024.118989

Zhang Y, Gu X, Rusk B, Mao W, Wang J, Zheng S (2022). In Situ Trace Elements in Quartz and K-Feldspar from Felsic Igneous Rocks: A Titanium-in-K-Feldspar Geothermometer for Natural Magmatic Systems. *Journal of Petrology* 63(11). doi:10.1093/petrology/egac113